9314–9336 *Nucleic Acids Research, 2023, Vol. 51, No. 17* *Published online 13 July 2023*
https://doi.org/10.1093/nar/gkad584

mRNA decapping activators Pat1 and Dhh1 regulate transcript abundance and translation to tune cellular responses to nutrient availability

Anil Kumar Vijjamarri[1,†], Neha Gupta[1,†], Chisom Onu[2], Xiao Niu[3], Fan Zhang[1], Rakesh Kumar[1], Zhenguo Lin[3], Miriam L. Greenberg[2] and Alan G. Hinnebusch[1,*]

[1]Division of Molecular and Cellular Biology, *Eunice Kennedy Shriver* National Institute of Child Health and Human Development, National Institutes of Health, Bethesda, MD 20892, USA, [2]Department of Biological Sciences, Wayne State University, Detroit, MI, USA and [3]Department of Biology, Saint Louis University, St. Louis, MO 63103, USA

Received February 12, 2023; Revised June 17, 2023; Editorial Decision June 19, 2023; Accepted July 10, 2023

ABSTRACT

We have examined the roles of yeast mRNA decapping-activators Pat1 and Dhh1 in repressing the translation and abundance of specific mRNAs in nutrient-replete cells using ribosome profiling, RNA-Seq, CAGE analysis of capped mRNAs, RNA Polymerase II ChIP-Seq, and TMT-mass spectrometry of mutants lacking one or both factors. Although the Environmental Stress Response (ESR) is activated in *dhh1Δ* and *pat1Δ* mutants, hundreds of non-ESR transcripts are elevated in a manner indicating cumulative repression by Pat1 and Dhh1 in wild-type cells. These mRNAs show both reduced decapping and diminished transcription in the mutants, indicating that impaired mRNA turnover drives transcript derepression in cells lacking Dhh1 or Pat1. mRNA degradation stimulated by Dhh1/Pat1 is not dictated by poor translation nor enrichment for suboptimal codons. Pat1 and Dhh1 also collaborate to reduce translation and protein production from many mRNAs. Transcripts showing concerted translational repression by Pat1/Dhh1 include mRNAs involved in cell adhesion or utilization of the poor nitrogen source allantoin. Pat1/Dhh1 also repress numerous transcripts involved in respiration, catabolism of non-preferred carbon or nitrogen sources, or autophagy; and we obtained evidence for elevated respiration and autophagy in the mutants. Thus, Pat1 and Dhh1 function as post-transcriptional repressors of multiple pathways normally activated only during nutrient limitation.

GRAPHICAL ABSTRACT

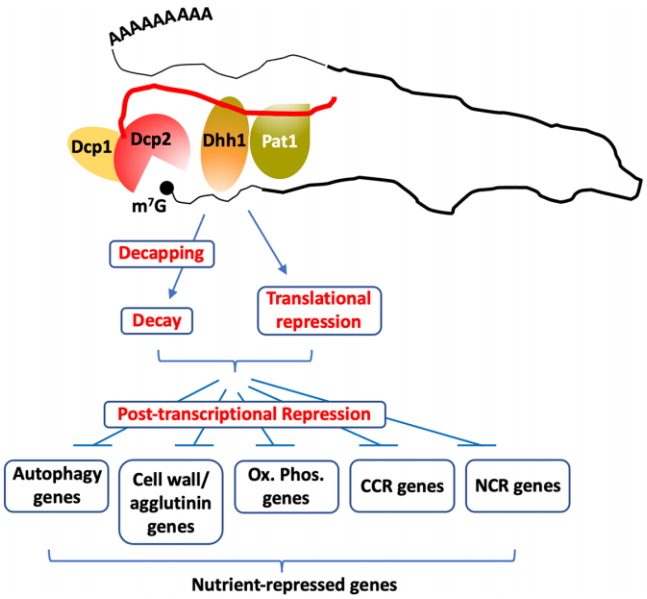

INTRODUCTION

Degradation of mRNA can be regulated in response to nutrient availability, cell stress, and developmental pathways in eukaryotic cells and it also serves to eliminate aberrant mRNAs unable to produce the correct proteins. Two major pathways of mRNA turnover have been identified in budding yeast involving exonucleolytic degradation from either the 5′ or 3′ end of the mRNA, both initiated by truncating the poly(A) tail. The deadenylated mRNAs can be degraded from the 3′ end by the exosome complex or from the 5′ end by Xrn1 following removal of the m^7G cap by the Dcp1/Dcp2 decapping enzyme. Decapping is activated

*To whom correspondence should be addressed. Tel: +1 301 496 4480; Email: ahinnebusch@nih.gov
†The authors wish it to be known that, in their opinion, the first two authors should be regarded as Joint First Authors.
Present address: Neha Gupta, GSK, Rockville, MD 20850, USA.

by various factors that interact with the C-terminal tail (CTT) of the catalytic subunit, Dcp2, including Edc3, Scd6, DEAD-box helicase Dhh1 and Pat1 protein (1). There is evidence that Pat1 is recruited to oligoadenylate tails produced by partial deadenylation, in association with the Lsm1-Lsm7 complex, and activates decapping via direct interactions with Edc3, Dhh1, and Dcp2 itself via different segments of Pat1 (2,3). The fact that Dcp2 and Xrn1 both bind the Pat1 CTD suggests a role for Pat1 in organizing sequential mRNA decapping and 5′ to 3′ degradation (2). Recent findings suggest that recruitment of Dhh1 to Dcp1/Dcp2 is mediated interchangeably by Edc3 or Scd6 bound to the same segment of the Dcp2 CTT, that Xrn1 is also recruited by the CTT, and that Edc3 and Xrn1 are constituents of alternative complexes assembled by Dcp1/Dcp2 that variously contain Scd6, Dhh1, or Pat1 (4).

Genome-wide analysis of mRNA abundance (RNA-Seq) in yeast mutants lacking Dhh1, Pat1, or Lsm1 in rich medium revealed a high degree of overlap (∼85–90%) in the sets of mRNAs whose relative abundance increased (∼1000 mRNAs) or decreased (∼700 mRNAs) in *pat1Δ* or *lsm1Δ* mutants versus wild-type (WT), consistent with Pat1 functioning in mRNA decay in a complex with Lsm1-7. Lesser overlaps (∼40–50%) were found for the up-and down-regulated mRNAs identified in *dhh1Δ* versus *pat1Δ* or *lsm1Δ* cells. These findings suggested that specific subsets of mRNAs are preferentially targeted by either Pat1/Lsm1-7 or Dhh1 for enhanced mRNA turnover, while also revealing functional cooperation between these factors in controlling the abundance of other mRNAs (5).

It has been established that certain glucose-repressed mRNAs are more rapidly degraded on addition of glucose to cells growing in a non-fermentable carbon source (6) and both Dhh1 and Xrn1 have been implicated in this response (7,8). Dhh1 is also involved in destabilizing a subset of *ATG* gene transcripts in nutrient-rich medium, whose products function in autophagy, helping to restrict autophagy to starvation conditions (9). Interestingly, rather than promoting mRNA decay, Pat1 appears to protect certain *ATG* transcripts from degradation by the exosome in nitrogen-starved cells (10).

In addition to regulating mRNA degradation, there is evidence that Pat1 and Dhh1 have overlapping functions in repressing mRNA translation at the initiation step in glucose- or amino acid-starved cells (11–13). Moreover, overexpression of Dhh1 or Pat1 can impede bulk translation initiation in non-starved cells, and each protein can reduce assembly of 48S preinitiation complexes (PICs) when added to yeast extracts (12). Pat1 can interact with 40S subunits (14) and with mRNP complexes containing initiation factors eIF4E/eIF4G and poly(A) binding protein Pab1 (15), which could be instrumental in inhibiting initiation. There is also evidence that Pat1 expressed at native levels stimulates, rather than represses, bulk translation initiation in non-starved cells and in cell extracts (14).

Tethering Dhh1 to a reporter transcript accelerates mRNA degradation, dependent on Dcp1/Dcp2, but also represses translation when the reporter mRNA is stabilized in mutants lacking decapping activity (16,17). Tethering Dhh1 shifts reporter mRNA to larger polysomes, suggesting a reduced rate of translation elongation, and native Dhh1 was found associated with polysomes under conditions of impaired elongation. Dhh1 has been implicated in mediating accelerated mRNA degradation associated with non-optimal codons in yeast mRNAs (18) and is required for the rapid degradation conferred by inserting suboptimal codons in reporter mRNA (16). Evidence suggests that a queue of slowly elongating ribosomes upstream from non-optimal codons triggers Dhh1-mediated mRNA turnover, and that overexpressing or tethering Dhh1 leads to ribosome stalling during elongation at non-optimal codons. Moreover, Dhh1 association was found to correlate with codon non-optimality for many native mRNAs (19). These results suggest Dhh1 binds to ribosomes slowly elongating through non-optimum codons and triggers their decapping and degradation. Structural evidence suggests that ribosomes stalled at suboptimal codons with an empty A site are recognized by Not5 binding to the ribosomal E-site to elicit Dhh1 recruitment and increased mRNA decapping and degradation (20). Dcp2, Pat1 and the deadenylase subunits of the Ccr4/Not complex appear to contribute to the same process (19,21).

Several ribosome profiling studies of *dhh1Δ* mutants have identified hundreds of mRNAs that appear to be translationally repressed or activated by Dhh1 in nutrient-replete cells (19,22,23), but it is unclear whether codon optimality is a strong determinant of translational repression by Dhh1 throughout the translatome. Indeed, one study found that mRNAs exhibiting changes in translation efficiency (TE) on elimination of Dhh1 generally did not exhibit changes in mRNA abundance, inconsistent with parallel functions of Dhh1 in repressing translation and activating mRNA turnover on the same mRNAs. Evidence of translational repression at the elongation step was also lacking from the analysis of ribosome densities across CDSs in *dhh1Δ* versus WT cells. Transcripts translationally stimulated by Dhh1 tended to have heightened propensity for structure in the beginning of the CDS and 5′UTRs, suggesting that Dhh1 might activate translation by unwinding structures in the beginning of CDSs (22). Interestingly, while acting in nutrient-replete cells to repress the abundance of a subset of *ATG* mRNAs (9), Dhh1 promotes autophagy in starved cells by stimulating translation of *ATG1* and *ATG13* mRNAs, dependent on its helicase activity and sequences in the 5′ ends of the CDS predicted to form secondary structures (24).

In this study, we used ribosome profiling to determine the genome-wide effects on translation of eliminating Pat1 in nutrient-replete cells. In view of previous findings that Pat1 and Dhh1 are partially redundant for repressing bulk translation in glucose-starved cells, we also analyzed a *pat1Δdhh1Δ* double mutant and compared the results to those we determined previously for an isogenic *dhh1Δ* mutant under identical culture conditions (23). RNA-Seq analysis of the three mutants revealed that Pat1 and Dhh1 generally make cumulative contributions to repressing the abundance of target mRNAs; and parallel sequencing of the capped fractions of all mRNAs suggests that decapping is a key driver of mRNA repression by both factors. While the results support the model that Pat1 and Dhh1 independently stimulate decapping by Dcp1/Dcp2, the two proteins frequently target the same mRNAs for enhanced

degradation. Our Ribo-Seq data reveal the functional interplay between Pat1 and Dhh1 in translational control, identifying mRNAs that are repressed primarily by one or the other protein, while also identifying cooperation between these factors in achieving strong translational repression of a set of poorly translated mRNAs. Proteomic analysis suggests that Dhh1- and Pat1-mediated translational repression generally targets the initiation stage of protein synthesis. Interestingly, we uncovered cooperation by Pat1 and Dhh1 in repressing the abundance or translation of numerous transcripts whose products function in respiration, the catabolism of non-preferred carbon or nitrogen sources, in autophagy, or in cell adhesion—all pathways normally repressed on rich medium. Thus, Dhh1 and Pat1 emerge as important post-transcriptional regulators that help to adjust gene expression to the quality and quantity of key nutrients.

MATERIALS AND METHODS

Yeast strains and plasmids

The following yeast strains were employed for all experiments: WT strain F2147 (W303) (*MATa ade2-1 ura3-1 his3-11,15 trp1-1 leu2-3 112 can1-100*), *dhh1Δ* strain H5217 (*MATa ade2-1 ura3-1 his3-11,15 trp1-1 leu2-3 112 can1-100 dhh1Δ::kanMX*), *pat1Δ* strain F2181 (*MATa ade2-1 ura3-1 his3-11,15 trp1-1 leu2-3 112 can1-100 pat1Δ::HIS3*), and *pat1Δdhh1Δ* strain F2182 (*MATa ade2-1 ura3-1 his3-11,15 trp1-1 leu2-3 112 can1-100 pat1Δ::HIS3 dhh1Δ::kanMX*).

The plasmids used in this study are listed in Table S1. Plasmids pNG162 and pNG164 contain the *PAT1* CDS, with 500 bp upstream and 192 bp downstream, on a 3083 bp fragment amplified by PCR from yeast genomic DNA, and inserted between the SalI and XmaI sites of YCplac111 or YCplac33, respectively. The plasmids were constructed by NEBuilder HiFi DNA assembly (New England Biolabs) according to the manufacturer's protocol and the inserted yeast DNA fragments were sequenced in their entirety

pRK4 was constructed by inserting sequences modified from the 5′-noncoding region of *MEP2* to introduce additional GATA sequences to the existing UAS region, PCR-amplified from genomic DNA of WT strain W303 using primers MEP2-*Sal*I FP (5′ GGGCTGCGTCGACAGATAAGGAACAAATGGATAAGGTCTTTAAG 3′) and MEP2-*Xho*I RP (5′ CCTCTTGTCTCGAGCTTATCATTGATAAGGCACAGGGTCTTATCACGCCGCT 3′). The amplified product was digested with SalI and XhoI and inserted into a derivative of pLG669Z lacking the XhoI fragment digested with the same restriction enzymes. The inserted fragment was confirmed by DNA sequencing.

nLUC reporters were constructed for 27 different genes (listed in File S1) to fuse the nanoLUC coding sequences (codon-optimized for *S. cerevisiae* (see File S2), preceded by the GGG codon for glycine) to the last codon of the complete CDS of each gene, preserving the native stop codon, 3′UTR sequences, and segment of 3′-noncoding sequences of the gene, as well as a segment of 5′-noncoding sequences including the native promoter and 5′UTR sequences of the gene of interest, by the following three-step procedure. First, DNA fragments were synthesized containing a SmaI site, the nanoLUC CDS (including the ATG and stop codon), the native stop codon and 3′ non-coding sequences for each gene of interest, and an EcoRI site, and inserted between the SmaI and EcoRI sites of pRS316 to produce an intermediate plasmid for each gene of interest. Second, PCR-amplification from WT yeast genomic DNA was conducted to generate a fragment for each gene of interest containing 20 nt of pRS316 adjacent to the SmaI site, the CCC nucleotides of the SmaI site, the 5′-noncoding region, 5′UTR, and CDS of the relevant gene (excluding the stop codon), the CCC complement of the GGG glycine codon, and the first 20nt of the nanoLUC CDS. Third, Gibson assembly was used to insert the PCR-amplified fragments from the second step at the SmaI sites of the intermediate plasmids, using 2× ExSembly Cloning Master mix (LifeSct LLC, Cat. M0005) and following the vender's instructions except that a 15 min incubation at 25°C was included prior to the 37°C incubation to allow for optimal SmaI digestion.

Cell spotting growth assays

Yeast transformants harboring plasmids containing *PAT1*, *DHH1* or empty vectors were grown to mid-logarithmic phase at 30°C in liquid synthetic complete medium (SC) without leucine or uracil, or lacking both (SC-L-U). Cultures were diluted to OD_{600} of 0.1 and 10-fold serial dilutions were spotted on agar medium of the same composition and incubated at 30°C or 37°C.

Polysome profiling

Polysome profiling was conducted as described previously (23) with the following modifications. Strains were cultured in YPD medium at 30°C to mid-logarithmic phase (OD_{600} of ∼0.5–0.6 for the WT and single mutants and ∼0.4 for the double mutant). Thirty OD_{260} units of cleared lysates were loaded onto 15–45% (w/w) sucrose gradients and centrifuged at 39 000 rpm for 2.5 h. Gradients were fractionated using the BioComp Gradient Station. Polysome to monosome (P/M) ratios were calculated using Fiji software.

Ribosome profiling

Ribosome profiling and RNA-seq were performed in parallel as described in (23), including use of Ribo-Zero Gold rRNA Removal Kit (Illumina, MRZ11124C), except that three biological replicates of each strain were analyzed and differential expression analysis of mRNA, RPF (Ribo reads) and TEs were conducted using DESeq2 (25), excluding genes with less than 128 total mRNA reads or 32 RPF reads in the 6 samples combined for each pairwise comparison of two strains. As in Zeidan *et al.* mutant and WT strains in the W303 strain background were cultured in YPD medium at 30°C to mid-logarithmic phase (OD_{600} of ∼0.6).

qRT-PCR analysis of mRNA abundance

Strains were grown as for ribosome profiling and total RNA was extracted by the hot-phenol method (26). Forty picograms of Luciferase Control RNA (Promega, L4561) was added to 1 μg of total RNA pre-treated with

DNase I (Roche, 4716728001), and 1 μg aliquots were used for cDNA synthesis using Superscript III First-Strand synthesis kit (Invitrogen, 18080051). qRT-PCR was carried out using 10-fold diluted cDNA and Brilliant II SYBR Green qPCR Master Mix (Agilent, 600828) with appropriate primer pairs (200 nM). Expression of each transcript was normalized to that of luciferase spike-in RNA from at least two biological replicates. Primers for qRT-PCR analysis of RNA expression are listed in Table S2.

CAGE sequencing and data analysis

(i) *CAGE library preparation and sequencing:*

CAGE sequencing and RNA-Seq were conducted in parallel on the same total RNA samples isolated from the same WT, *dhh1Δ* and *pat1Δ* strains, in duplicates, that were subjected to ribosome profiling, using hot-phenol extraction (26). RNA samples were quantified using a Nanodrop ND-1000 spectrophotometer (ThermoFisher) and evaluated for quality using the Bioanalyzer 2100 (Agilent Technologies). CAGE libraries were constructed from 5 μg of total RNA of each strain using the nAnT-iCAGE protocol (27) by K.K. DNAFORM of Japan. Briefly, first strand cDNAs were transcribed to the 5′ end of capped RNAs and attached to CAGE 'barcode' tags. Each nAnT-iCAGE library used linkers with specific barcodes and was sequenced using Illumina NextSeq500 (single-end, 75 bp reads). The numbers of reads generated from each library are listed in File S7.

(ii) *CAGE data processing, alignment, rRNA filtering and identification of TSSs and TCs:*

The sequenced CAGE reads of each sample were aligned to the reference genome of *S. cerevisiae* S288c (Assembly version: sacCer3) using HISAT2 (28). For read alignment, we disabled the soft clipping option in HISAT2 by using '–no-softclip' to avoid false-positive transcription start sites (TSSs). CAGE reads mapped to rRNA genes were identified using rRNAdust (http://fantom.gsc.riken.jp/5/sstar/Protocols:rRNAdust), and were excluded from subsequent TSS analyses. TSS identification, inference of TSS clusters (TC, representing putative core promoters), and assigning TCs to their downstream genes were carried out by using TSSr (29). CAGE reads with a mapping quality score (MAPQ) > 20 were considered uniquely mapped reads, which were used for subsequent analyses. CAGE signals of biological replicates were then merged as a single sample. The transcription abundance of each TSS was quantified as the numbers of CAGE tags (reads) supporting the TSS per million mapped reads (TPM). Only TSSs with TPM ≥0.1 were used to infer TSS clusters (TCs), representing putative core promoters. The 'peakclu' method (30) was used to infer TCs for each sample, with the following options 'peakDistance = 50, extensionDistance = 25, localThreshold = 0.01'. A set of consensus TCs for all samples were generated by using the 'consensusCluster' function in TSSr with an option of 'dis = 100'. Consensus TCs were then assigned to their downstream genes if they are within 1000 bp upstream and 50 bp downstream of the start codon of annotated ORFs (File S7). The TPM value of a consensus TC in a sample is the sum of TPM values of all TSSs within its range. The TPM value of a gene was calculated as the sum of all consensus TC assigned to the gene.

(iii) *RNA sequencing:*

RNA sequencing libraries were produced in parallel from the same total RNA samples subjected to CAGE sequencing by the NHLBI DNA sequencing Core at NIH (Bethesda, MD) using the TruSeq Stranded mRNA Library Prep Kit (Illumina, Paired-end 50 bp reads) and sequenced using the NovaSeq6000 Illumina platform. Prior to library preparation, rRNA was depleted using the QIAGEN FastSelect yeast rRNA depletion kit. Sequencing reads were mapped to the S288C genome (R64-1-1 S288C SacCer3) using STAR aligner (Dobin et al. 2013) and PCR duplicates were removed by Samtools. To calculate absolute mRNA changes between WT and mutant strains, ERCC ExFold RNA Spike-In mixes (Ambion, 4456739) were added in equal amounts (2.4 μl of 1:100 fold dilutions) to 1.2 μg of total RNA, adding Mix I to WT and Mix II to the mutant samples. Total ERCC reads obtained from the 23 spike-in transcripts belonging to subgroup B (present in equal concentrations in Mix I and Mix II) were used to calculate size factors for each library and reads corresponding to yeast genes were normalized by the size factors. DESeq2 was employed to calculate the differential expression between strains by setting the size factor to unity.

(iv) *Calculation of differentially expressed capped or total mRNAs from CAGE sequencing and RNA sequencing results:*

Differential expression in total RNA (ΔmRNA_T) or capped RNA (ΔmRNA_C) in *pat1Δ* or *dhh1Δ* versus WT cells was assessed by DESeq2 (25) based on raw read count from RNA-seq or CAGE sequencing.

(v) *Calculation of C/T ratios from CAGE sequencing and RNA sequencing results:*

RNA-Seq reads assigned to each gene were also normalized as transcripts per million reads (TPM). Because a single read/tag is generated for each transcript in CAGE, its TPM (tags per million mapped tags) is equivalent to TPM values in RNA-Seq, which makes the two types of TPM values comparable. The C/T ratio of each gene was calculated by dividing CAGE TPMs by RNA-Seq TPMs in each strain (WT, *pat1Δ* or *dhh1Δ*) after first removing all genes with zero CAGE reads in either the mutant or WT strain being compared. To measure the C/T ratios for particular groups of mRNAs dysregulated by *pat1Δ* or *dhh1Δ*, the RNA-Seq data obtained from the same RNA samples subjected to CAGE sequencing were analyzed by DESeq2 to define the upregulated (mRNA_up) or downregulated (mRNA_dn) groups for each mutation. Highly similar results were obtained if the RNA-Seq data obtained in parallel with ribosomal profiling were used instead to define these mRNA groups, as done in Figure 1.

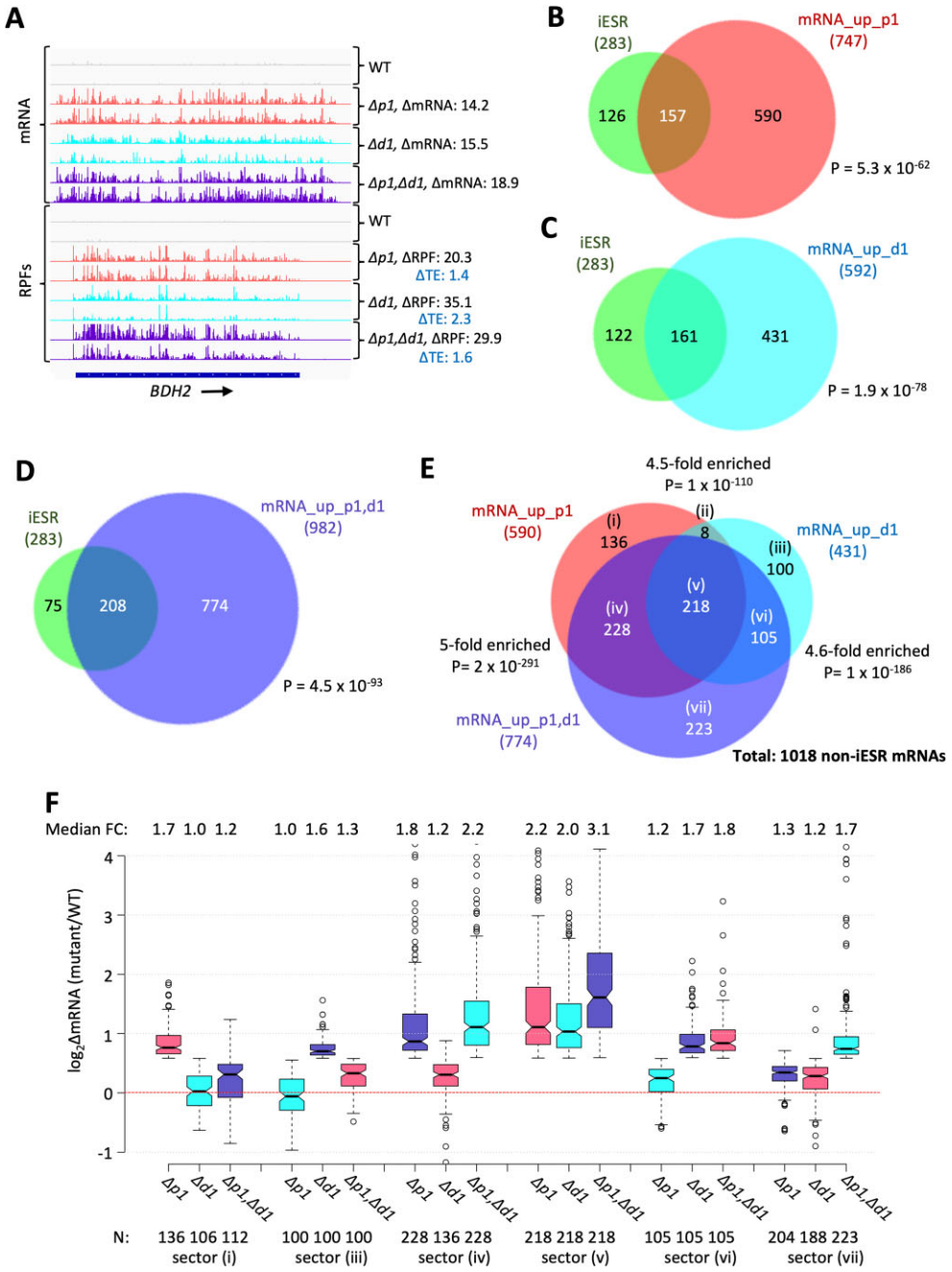

Figure 1. Most mRNAs dysregulated in abundance by *pat1Δ* or *dhh1Δ* exhibit cooperation between Pat1 and Dhh1 ranging from functional redundancy to interdependence. (**A**) Gene browser image showing the mRNA reads (top 8 tracks) and RPF reads (bottom 8 tracks) measured by ribosome profiling for two biological replicates of WT and the *pat1Δ* (*Δp1*), *dhh1Δ* (*Δd1*), or *pat1Δdhh1Δ* (*Δp1,Δd1*) mutants versus WT for *BDH2*, with the fold-changes in mRNA, RPFs or TEs between mutant and WT indicated to the right of each track. (**B**–**D**) Venn diagrams of the overlap between the mRNA_up groups identified in *pat1Δ, dhh1Δ* or *pat1Δdhh1Δ* mutants versus WT and the 283 induced ESR mRNAs. *P* values are indicated for the significance of overlaps determined by the hypergeometric distribution for the indicated total number (*N*) of expressed mRNAs in each mutant. (**E**) Venn diagrams of the overlap between all non-iESR mRNAs that are derepressed in abundance by the *pat1Δ, dhh1Δ* or *pat1Δdhh1Δ* mutations versus WT. Fold-enrichments and *P* values from the hypergeometric distribution are indicated for the overlapping sets. (**F**) Notched box-plot analyses of the $\log_2$ changes in mRNA abundance ($\log_2\Delta$mRNA) determined by DESeq2 analysis between the indicated mutants versus WT for the numbers of mRNAs (*N*) belonging to the specified sectors of the Venn diagram in (E). "Un-logged" median values are indicated at the top.

ChIP-seq and data analysis

WT, *dhh1Δ* and *pat1Δ* strains were cultured in triplicate in YPD medium to A_{600} of 0.6–0.8, treated with formaldehyde and subjected to ChIP-Seq as described (31) using monoclonal antibody against Rpb1 (8WG16, Biolegend, 664906). DNA libraries for Illumina paired-end sequencing were prepared using the DNA Library Prep Kit for Illumina from New England Biolabs (E7370L). Paired-end sequencing (50 nt from each end) was conducted by the DNA Sequencing and Genomics core facility of the NHLBI, NIH. Sequence data were aligned to the SacCer3 version of the genome sequence using Bowtie2 (32) with parameters -X 1000 -very-sensitive, to map sequences up to 1 kb with maximum accuracy. PCR duplicates from ChIP-Seq data were removed using the samtools rmdup package. Numbers of aligned paired reads from each ChIP-Seq experiment are summarized in File S8. Raw genome-wide occupancy profiles for Rpb1 were computed using the coverage function in R and relative occupancies were obtained by normalizing each profile to the average occupancy obtained for the relevant chromosome (https://github.com/rchereji/bamR). To visualize specific loci, BigWig files of samples were loaded in the Integrative Genomics Viewer (IGV) (33).

For spike-in normalization of Rpb1 ChIP-Seq data, identical aliquots of *S. pombe* chromatin were added to each *S. cerevisiae* chromatin sample being analyzed in parallel, corresponding to 10% of the DNA in the *S. cerevisiae* chromatin samples, prior to immunoprecipitating with Rpb1. As described fully in File S8, a normalization factor for each sample was calculated by dividing the average number of total *S. pombe* Rpb1 reads obtained across all samples by the total *S. pombe* reads obtained for that sample. The observed Rpb1 reads mapping to the *S. cerevisiae* genome were multiplied by the normalization factor to yield the spike-in normalized reads for that sample. Raw genome wide occupancy profiles for Rpb1 were computed using the coverage function in R, wherein each profile was set with the same total 'OCC' to allow the comparison between WT and mutant strains, using the custom R script (https://github.com/hzhanghenry/OccProR).

TMT-MS/MS analysis of global protein abundance

Replicate cultures of WT, *dhh1Δ, pat1Δ* and *dhh1Δpat1Δ* strains were cultured in YPD medium for ∼3 doublings to A_{600} of ∼0.6, and harvested by centrifugation for 5 min at 3000 × *g*. Cells were resuspended in nuclease-free water, collected by centrifugation, and stored at −80°C. WCEs were prepared in freshly prepared 8 M urea, 25 mM triethylammonium-bicarbonate (TEAB; Thermo Scientific, 90114) by washing the cell pellets once and resuspending again in the extraction buffer, then vortexing with glass beads in the cold room. Lysates were clarified by centrifugation at 13 000 × *g* for 30 min and the quality of extracted proteins was assessed following SDS-PAGE using GelCode™ Blue Stain (Thermo Scientific, 24592) and quantified with the Pierce™ BCA Protein Assay Kit (Thermo Scientific, 23225). Lysates were stored at −80°C. Sample preparation and TMT-MS/MS (34) was performed at the NHLBI Proteomics Core at NIH (Bethesda, MD) for the WT, *dhh1Δ,* and *pat1Δ* strains, and at the IDeA National Resource for Quantitative Proteomics for the *pat1Δdhh1Δ* and WT strains. At NHLBI, 100 μg of WCEs were incubated for 1 h at 37°C with freshly prepared 20 mM dithiothreitol (DTT) to reduce disulfide bridges. Alkylation was performed at room temperature (RT) for 1 h with freshly made 50 mM iodoacetamide in 25 mM ammonium bicarbonate and the reaction was quenched by adding DTT to 50 mM. Lysates were diluted 10-fold with 25 mM ammonium bicarbonate and digested with 3 μg of trypsin (Promega, v5111) overnight at 37°C. Digests were acidified by adding formic acid to 1% and desalted with Waters Oasis HLB 1cc columns. Peptides were eluted from desalted samples with 1 ml of buffer E (0.1% formic acid in 50% acetonitrile) and dried in a SpeedVac. Samples were labelled with TMT reagents for multiplexing (TMT10plex label reagent set, Thermo Scientific) according to the manufacturer's instructions. Briefly, resuspended TMT reagent was added to each sample, incubated for 1 h at RT and the reaction was quenched by adding 8 μl of 5% hydroxylamine and incubating for 15 min. To increase the protein coverage, each set of pooled TMT samples was separated into 24 fractions using basic reverse phase liquid chromatography (bRPLC). Quantification of TMT-labelled peptides was conducted on an LTQ Orbitrap Lumos-based nanoLCMS system (Thermo Scientific) with a 2 h gradient at 120k resolution for MS1 and 50K for MS2 at 38% HCD energy. Raw data was processed using Proteome Discoverer 2.4 (Thermo Scientific) and the MS2 spectra were searched in the SwissProt Yeast database (https://www.uniprot.org/proteomes/UP000002311) using the SEQUEST search engine (Eng *et al.* 1994). Peptide spectral matches (PSM) were validated using Percolator based on *q*-values at a 1% false discovery rate (Brosch *et al.* 2009) (http://www.sanger.ac.uk/Software/analysis/MascotPercolator/). Relative abundance of each peptide in a strain is measured by normalizing to the total abundance of that peptide coming from all the strains used in the study. We determined the protein-level fold changes based on the median of peptide-level fold changes from the Proteome Discoverer-produced abundances.

Analysis of *nLUC* reporter expression

Yeast transformants harboring *nLUC* reporter plasmids were cultured overnight at 30°C in SC-Ura, diluted to OD_{600} of 0.1, and cultured to OD_{600} of 1.0–1.5. WCEs were prepared in phosphate-buffered saline (PBS) containing 1 mM PMSF and protease inhibitor cocktail (Roche, 5056489001) by vortexing with glass beads, and clarified by centrifugation at 13 000 × *g* for 30 min at 4°C. Luciferase assays were conducted using Nano-Glo® Luciferase Assay Substrate and Nano-Glo® Luciferase Assay Buffer (Promega, N1120) following the instructions provided by the vendor and bioluminescence was determined immediately using a Centro Microplate Luminometer (Berthold). Relative light units were normalized to total protein abundance in the WCEs determined using the Bradford reagent (BioRad, 5000006).

Western blot analysis

WCEs were prepared by trichloroacetic acid extraction as previously described (35) and immunoblot

analysis was conducted as described previously (36). After electroblotting to nitrocellulose membranes (Bio-Rad 1620094), membranes were probed with antibodies against Atp20, Cox14, Pet10, Qcr8, Sdh4 (kindly provided by Dr. Nikolaus Pfanner), Cyb2 (kindly provided by Dr. Thomas Fox), Idh1 (Abnova, PAB19472), Cit2 (Antibodies-online.com, ABIN4889057), and Gcd6 (37). Secondary antibodies employed were HRP-conjugated anti-rabbit (Cytiva, NA9340V), anti-mouse IgG (Cytiva, NA931V) and anti-goat IgG (Abnova, PAB29101). Detection was performed using enhanced chemiluminescence (ECL) Western Blotting Detection Reagent (Cytiva, RPN2016) and the Azure 200 gel imaging biosystem. NIH ImageJ was employed to analyze images for quantification.

Measuring mitochondrial membrane potential

Precultures were grown in SC-Ura (to select for the *URA3* plasmids) to OD_{600} of ∼3.0 and used to inoculate YPD medium at OD_{600} of 0.2. Cells were grown to OD_{600} of ∼0.6–0.8 and incubated with 500 nM TMRM for 1 h. Cells were washed once with distilled H_2O and fluorescence was measured using flow cytometry (BD LSR II) at the Microscopy, Imaging & Cytometry Resources (MICR) Core at Wayne State University. Dye fluorescence is proportional to mitochondrial membrane potential. Median fluorescence intensity (MFI) of single cells was analyzed with the FlowJo software, and normalized to the OD_{600} of the cultures. Data presented are in arbitrary fluorescence units normalized to OD_{600} of the cultures. In control samples, 50 μM FCCP was added to cells to dissipate the membrane potential and provide a measure of non-specific background fluorescence.

Assay of autophagy

Expression and cleavage of the GFP-Atg8 fusion protein in different strains was conducted as previously described (24). Strains were cultured in SC-U to OD_{600} of 0.5 to select for the *GFP-ATG8* plasmid pRS416GFP-ATG, harvested by centrifugation, resuspended in YPD and grown for one doubling. For nitrogen starvation of the WT strain, cells were grown to mid-logarithmic phase in SC-U, harvested, and resuspended in nitrogen starvation medium (SD-N; SD prepared with 0.17% yeast nitrogen base without ammonium sulfate and amino acids) and incubated for 3 h.

Data visualization and statistical analysis

Notched box-plots were constructed using a web-based tool at http://shiny.chemgrid.org/boxplotr/. In all such plots, the upper and lower boxes contain the 2nd and 3rd quartiles and the band gives the median. If the notches in two plots do not overlap, there is roughly 95% confidence that their medians are different. Scatterplots displaying correlations between sequencing read counts from biological replicates were created using the scatterplot function in Microsoft Excel and density scatter plots were created using ggplot2 function in R. Pearson's correlation analysis and the Student's *t*-test were conducted using Microsoft Excel. Venn diagrams were generated using the web-based tool https://www.biovenn.nl/ and the significance of gene set overlaps in Venn diagrams was evaluated with the hypergeometric distribution using the web-based tool https://systems.crump.ucla.edu/hypergeometric/index.php. Hierarchical clustering analysis was conducted with the R heatmap.2 function from the R 'gplots' library, using the default hclust hierarchical clustering algorithm. Gene ontology (GO) analysis was conducted using the web-based tool at http://funspec.med.utoronto.ca/.

RESULTS

Pat1 and Dhh1 functionally cooperate to control the abundance of many mRNAs independently of the ESR

In this study we have analyzed isogenic *pat1Δ, dhh1Δ* and *pat1Δdhh1Δ* mutants, all exhibiting slow-growth (Slg^-) phenotypes, particularly at 37°C, that could be complemented by the WT alleles on plasmids (Supplemental figure Figure S1A). Analysis of bulk polysome assembly revealed a ∼25% reduction in polysomes to monosomes (P/M) in the *pat1Δ* mutant, which increased to ∼40% in the double mutant (Figure S1B). These results are consistent with previous findings that *pat1Δ* reduced bulk translation initiation (14). The greater reduction in polysomes in the double mutant coupled with the ∼WT P/M ratio in *dhh1Δ* cells suggests that Dhh1 promotes translation in a manner largely masked by Pat1, indicting functional redundancy between the two factors.

To determine the effects of the mutations on abundance and translation of individual mRNAs, we conducted RNA-Seq and ribosome profiling (Ribo-Seq) of the mutant and WT strains growing exponentially in YPD medium at 30°C. Ribo-Seq entails deep-sequencing of ribosome-protected fragments (RPFs, or ribosome footprints), and the ratio of RPF reads to total mRNA reads determined by RNA-Seq summed over the coding sequences (CDS) provides a measure of relative translational efficiency (TE) for each mRNA (38). The ribosome footprint and RNA-Seq data for each gene among biological replicates of each strain were highly reproducible, with Pearson correlation coefficients of 0.99. Analysis of the RNA-Seq data by DESeq2 (25) identified 747 mRNAs significantly derepressed in the *pat1Δ* mutant versus WT by > 1.5-fold at a false discovery rate (FDR, p-value adjusted for multiple hypothesis testing) of < 0.05 (dubbed mRNA_up_p1); and a group of 600 mRNAs down-regulated by the same fold-change and FDR (mRNA_dn_p1). Our previous RNA-Seq results for the *dhh1Δ* strain obtained using the same experimental conditions and methodology (23) identified comparable groups of up-regulated (mRNA_up_d1) or down-regulated mRNAs (mRNA_dn_d1) in *dhh1Δ* versus WT cells. Interestingly, the *pat1Δdhh1Δ* double mutation conferred up- and down-regulation of 982 and 1052 mRNAs, groups ∼1.3-fold and ∼1.7-fold larger than those dysregulated by *pat1Δ,* respectively. (All transcripts in the mRNA_up and mRNA_dn groups are provided in File S4). *BDH2* is a representative gene showing mRNA derepression in replicates of all three mutants (Figure 1A). Importantly,

qRT-PCR analysis revealed changes in mRNA abundance for 12 different transcripts in both *dhh1Δ* and *pat1Δ* mutants well-correlated with their changes in RNA-Seq (Figure S2A-D) (File S3).

The *pat1Δ* and *dhh1Δ* strains belong to a large group of slow-growing yeast mutants exhibiting the Environmental Stress Response (39) involving induction of ∼300 mRNAs (iESR transcripts) and repression of ∼600 others (rESR) in various stresses, with the rESR group dominated by ribosomal protein (RP) or ribosome biogenesis (RiBi) genes (40) (File S4). As expected, all three mutants show significant increases in median mRNA abundance of iESR mRNAs and decreases in rESR transcripts, comparable to those conferred by the slowest-growing yeast mutants (Figure S3A, B). (In this and other box plots, nonoverlapping notches for adjacent boxes indicates that their medians differ with 95% confidence; and if notches do not overlap 0 in log(2) plots, the median differs from that for all mRNAs, which will be close to unity). Although > 50% of iESR mRNAs are derepressed in all three mutants, ∼73–79% of the mRNAs up-regulated in the mutants are not iESR transcripts (Figure 1B–D), consistent with a more direct role for Pat1 and Dhh1 in targeting these mRNAs for degradation. The mRNAs down-regulated in the mutants, again most of which are not rESR transcripts, might undergo more rapid degradation mediated by other activators of Dcp1/Dcp2 or by the exosome in cells lacking Pat1/Dhh1, as suggested previously (5). In subsequent analyses of mRNA changes, we excluded all ESR mRNAs to focus on transcripts controlled directly by Pat1 and Dhh1.

There is a significant overlap between the non-iESR mRNAs derepressed in the *pat1Δ* or *dhh1Δ* single mutants (Figure 1E (ii) & (v)), in agreement with previous findings that Pat1 and Dhh1 cooperate in repressing certain mRNAs (5). While ∼70–75% of transcripts up-regulated in the single mutants were also upregulated in the double mutant, a sizeable group was derepressed only in the double mutant (Figure 1E(vii)), consistent with redundant functions of Pat1 and Dhh1 in repressing the latter transcripts. About 20% of mRNAs were derepressed in only one single mutant (Figure 1E(i) & (iii)), suggesting that they are controlled exclusively by Dhh1 or Pat1. Summing up all mRNAs in Figure 1E suggests that Dhh1 and Pat1 preferentially repress 1018 non-iESR mRNAs. A parallel analysis of transcripts down-regulated in the mutants reveals cooperation between Pat1 and Dhh1 in stimulating the expression of 1067 non-rESR mRNAs (Figure S3C).

Examining the mRNA changes for the transcripts up-regulated in all three mutants (Figure 1E(v)), reveals a cumulative effect of combining *pat1Δ* and *dhh1Δ* that increases the median derepression in the double mutant above that in either single mutant compared to WT (Figure 1F(v)). A similar situation applies to the mRNAs derepressed only in the double mutant, for which both single mutations confer smaller increases versus the double mutation (Figure 1E, F(vii)). Evidence of cumulative derepression is also evident for the mRNAs up-regulated in *pat1Δ* and *pat1Δdhh1Δ* mutants but not in *dhh1Δ* cells (Figure 1E (iv)), which appeared to be independent of Dhh1, but actually show derepression in the *dhh1Δ* mutant merely to a smaller degree than in the other two mutants (Figure 1F(iv)). The same holds for the corresponding mRNAs ostensibly independent of Pat1, which exhibit modest derepression in *pat1Δ* cells but strong derepression in *dhh1Δ* cells and the double mutant (Figure 1E-F(vi)). Thus, for ∼76% of the mRNAs up-regulated in any one of the three mutants, Pat1 and Dhh1 both repress mRNA abundance and differ only in the magnitude of their contributions for particular mRNAs. For the remaining ∼24% of transcripts up-regulated in only one of the single mutants (Figure 1E(i) & (iii)), the median abundance is not increased in the other single mutant and is elevated to a smaller degree in the double mutant (Figure 1F(i) & (iii)). These last mRNAs are therefore repressed exclusively by Pat1 or Dhh1 in WT cells and the other factor appears to enhance rather than repress their abundance when Pat1 or Dhh1 is absent. One explanation for the latter would be if eliminating both Pat1 and Dhh1 simultaneously enables an alternative decay mechanism that lowers their abundance beyond that conferred by Pat1 or Dhh1 in WT cells.

Having RNA-Seq data on both *pat1Δ* single and *pat1Δdhh1Δ* double mutants allowed us to employ DESeq2 to identify mRNAs significantly changed in response to *dhh1Δ* only in cells lacking Pat1 (ie. comparing *dhh1Δpat1Δ* to *pat1Δ* cells). Using the statistical criteria described above, we identified 178 non-iESR mRNAs that were derepressed by eliminating Dhh1 in *pat1Δ* cells and were not similarly up-regulated on eliminating Dhh1 from WT cells (Figure S4A(i)). Similarly, 245 mRNAs were up-regulated > 1.5-fold by *pat1Δ* in cells containing *dhh1Δ* but not in *DHH1* cells (Figure S4C(i)) (mRNAs listed in File S5). As might be expected, these new mRNA groups display functional redundancy in showing marked derepression only in the double mutants (Figures S4E, F). Adding such 'conditionally' Pat1- or Dhh1-repressed mRNAs to the transcripts derepressed in the single mutants produced combined groups of 609 non-iESR mRNAs up-regulated by *dhh1Δ*, dubbed mRNA_up_d1_c (Figure S4A) and 835 mRNAs derepressed by *pat1Δ* (mRNA_up_p1_c, Figure S4C). (Table 2 summarizes all transcript groups identified in this study). We similarly identified combined groups of non-rESR mRNAs down-regulated by *dhh1Δ* or *pat1Δ* (Figure S4B, D) (listed in File S5). Below, we analyze the properties of these more comprehensive groups of Dhh1- or Pat1-controlled transcripts.

Cluster analysis of the mRNA changes for the combined groups of regulated transcripts (Figure 2A) reveals that most Dhh1-controlled mRNAs changed their abundance in the same direction in the *dhh1Δ* and *pat1Δdhh1Δ* mutants versus WT (Spearman's $\rho = 0.84$), whereas the changes conferred by *pat1Δ* were less correlated ($\rho = 0.68$). Similar conclusions emerged from cluster analysis of the combined Pat1-controlled mRNAs (Figure 2B), with the majority changing concordantly in the *pat1Δ* and *pat1Δdhh1Δ* mutants versus WT ($\rho = 0.85$). Consistent with conclusions above, close inspection of the clustergrams indicates that most transcripts in the combined groups are regulated by both Dhh1 and Pat1, with *dhh1Δ* and *pat1Δ* mutations frequently conferring cumulative abundance changes, while a minority are controlled exclusively by Dhh1 or Pat1.

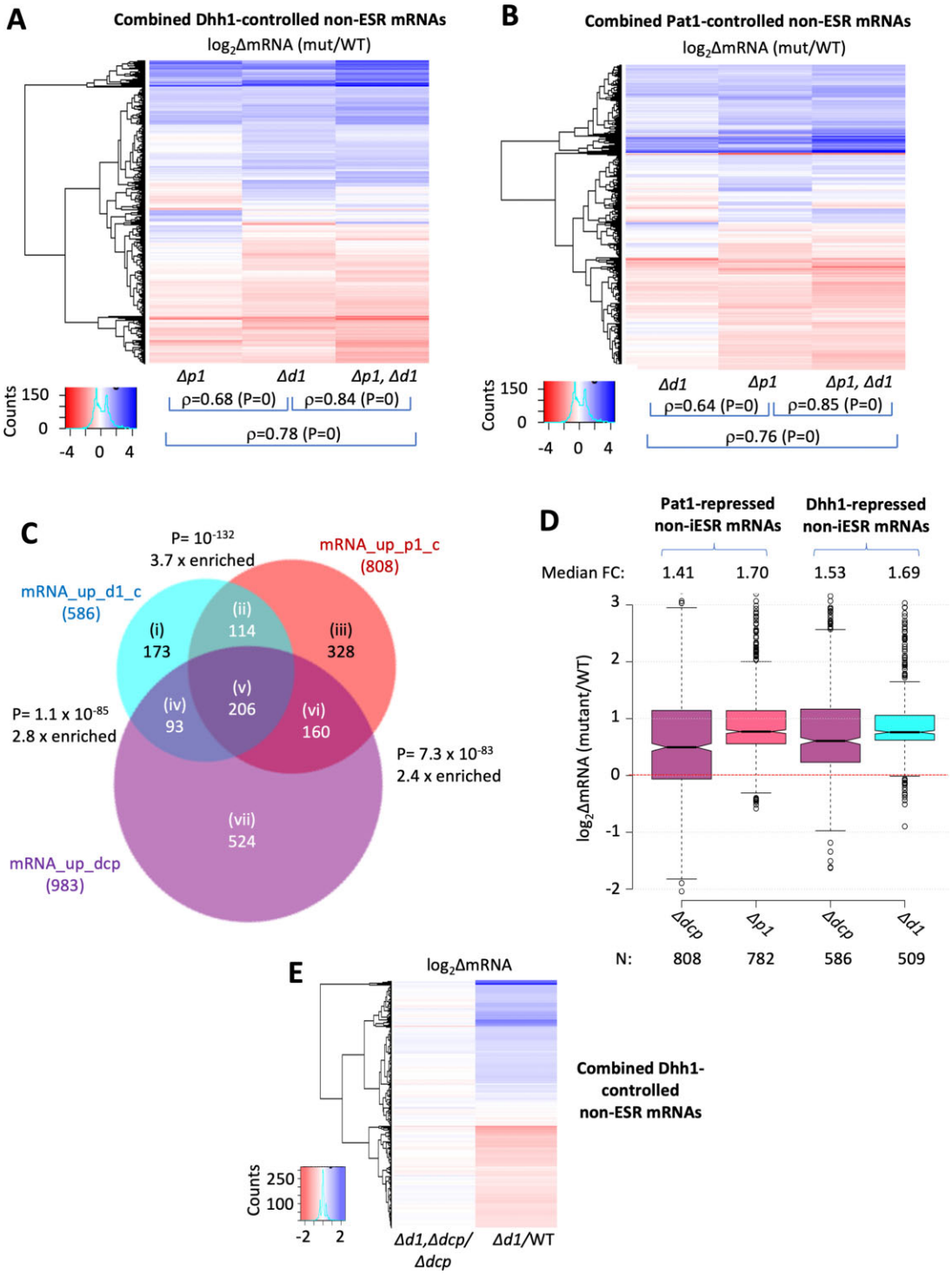

Figure 2. Many Dhh1- or Pat1-repressed mRNAs are targeted for degradation via decapping by Dcp1/Dcp2. (A, B) Hierarchical clustering analysis of $log_2\Delta$mRNA values determined by DESeq2 analysis conferred by the indicated mutations versus WT for 1023 of the 1141 mRNAs defined in Figure S4A and B that belong uniquely to the combined mRNA_up_d1_c or mRNA_dn_d1_c groups, for which RNA-Seq data was obtained in all four strains (**A**); or for 1267 of the 1457 mRNAs defined in Figure S4C and D that belong uniquely to the combined mRNA_up_p1_c or mRNA_dn_p1_c groups, with data in all three strains (**B**), conducted with the R heatmap.2 function from the R 'gplots' library, using the default hclust hierarchical clustering algorithm. Small numbers (10 or 11) of mRNAs were excluded with $log_2\Delta$mRNA values < -5 or > 5 to avoid skewing of color changes. Spearman coefficients and *P* values for the indicated correlation analyses are indicated. (**C**) Venn diagram of the overlap between the 983 non-iESR mRNAs derepressed by *dcp2Δ* by > 1.5-fold at FDR < 0.05 and the 586 and 808 mRNAs that belong uniquely to the mRNA_up_d1_c and mRNA_up_p1_c groups, respectively, defined in Figure S4A and C. Fold-enrichments and P values from the hypergeometric distribution are indicated for the overlaps between the three sets. (**D**) Notched box-plot analyses of the changes in mRNA abundance in the indicated mutants versus WT for mRNAs in the mRNA_up_p1_c group (cols. 1–2) and mRNA_up_d1_c group (cols. 3–4). (**E**) Hierarchical clustering analysis of $log_2\Delta$mRNA values conferred by *dhh1Δdcp2Δ* versus *dcp2Δ* (col. 1) and *dhh1Δ* versus WT (col. 2) for the combined Dhh1-controlled non-ESR mRNAs analyzed in (A).

Evidence that many Dhh1- or Pat1-controlled mRNAs are targeted for enhanced degradation via decapping by Dcp1/Dcp2

To determine whether the Dhh1- or Pat1-controlled mRNAs are similarly regulated by the decapping enzyme, we examined our previous RNA-Seq analysis of an isogenic *dcp2Δ* mutant compared to the same WT strain employed here, conducted under identical conditions (23). The 983 non-iESR mRNAs up-regulated by *dcp2Δ* (> 1.5-fold, FDR < 0.05), which should be enriched for transcripts targeted for degradation by decapping, overlapped extensively with the combined groups of mRNAs derepressed by *dhh1Δ* or *pat1Δ* (Figure 2C). Moreover, *dcp2Δ* increased the abundance of both Dhh1- and Pat1-repressed mRNAs to nearly the same degree as did *dhh1Δ* or *pat1Δ* (Figure 2D). These results support the possibility that a large proportion of mRNAs derepressed by *dhh1Δ* or *pat1Δ* are targeted by Dcp1/Dcp2 for enhanced decapping in WT. Further support for this came from evaluating the effects of *dhh1Δ* in the presence or absence of *DCP2,* by interrogating our previous RNA-Seq results from a *dhh1Δdcp2Δ* double mutant (File S6) (23). Importantly, *dhh1Δ* has little effect on the abundance of most Dhh1-controlled mRNAs in *dcp2Δ* cells, in contrast to the marked changes *dhh1Δ* confers in otherwise WT cells (Figure 2E). Thus, Dhh1 is dependent on Dcp2 for altering mRNA abundance in the manner expected if Dhh1 generally activates mRNA decapping.

There is evidence that mRNAs decapped by Dcp1/Dcp2 undergo 5′ to 3′ exonucleolytic decay co-translationally (41), with exonuclease Xrn1 'following behind' the last translating ribosomes loaded on the mRNAs prior to decapping (42). Such decapped intermediates may account for ∼12% of the polyadenylated mRNA population in WT cells (43). We reasoned that mRNAs targeted preferentially for decapping by Dhh1 or Pat1 should exhibit a greater than average proportion of decapped degradation intermediates in WT, which should be eliminated in the *dhh1Δ* or *pat1Δ* mutants owing to diminished decapping (Figure S5). To test these predictions, we carried out cap analysis of gene expression (CAGE) to sequence and quantify capped mRNA 5′ ends captured by biotinylation of the cap structure using the nAnT-iCAGE protocol (27). Biological replicates of both CAGE and standard RNA-Seq carried out in parallel on the same mRNAs from *dhh1Δ, pat1Δ* and WT strains were highly reproducible ($r > 0.9$) (File S7) and these new RNA-Seq data were highly correlated with the RNA-seq results obtained in parallel with Ribo-Seq ($r = 0.89$).

There are strong positive correlations between the changes in mRNA levels from RNA-Seq versus CAGE for both *dhh1Δ* and *pat1Δ* relative to WT ($r = 0.79$ & $r = 0.78$, respectivley) and DESeq2 analysis of both datasets revealed highly significant overlaps between capped versus total mRNAs upregulated by each mutation ($P = 3 \times 10^{-240}$ & 4×10^{-265}). These results are expected if most mRNAs derepressed by *dhh1Δ* or *pat1Δ* accumulate in the mutants as capped molecules. Recently, we made the same finding for mRNAs derepressed by *dcp2Δ*; however, we found a strong negative correlation for the *xrn1Δ* mutation (Vijjamarri *et al.* bioRxiv 2023.01.05.522830) expected from the fact that eliminating 5′ to 3′ degradation by Xrn1 should lead to accumulation of decapped intermediates versus capped molecules.

The transcript numbers from CAGE (C) and RNA-Seq (T) were determined for each gene (File S7) and the C/T ratios were calculated as a proxy for the proportion of capped molecules for each transcript (Because the CAGE and RNA-Seq data were normalized separately, the C/T ratios are relative, not absolute proportions of capped transcripts). Comparing C/T ratios between *dhh1Δ* and WT revealed that mRNAs exhibiting greater derepression of total transcript abundance in *dhh1Δ* versus WT cells (elevated T_d1/T_WT ratios) tend to show greater increases in the relative proportions of capped transcripts (elevated [C/T]_d1/[C/T]_WT ratios) between *dhh1Δ* and WT cells (Figure 3A). This correlation is expected if altered rates of decapping and degradation are important drivers of changes in transcript abundance in the mutant, but it would not be predicted if changes in mRNA levels arise indirectly from altered mRNA synthesis. Importantly, the C/T ratios are lower in WT cells for the mRNAs upregulated by *dhh1Δ* ('mRNA_T_up_d1') compared to all mRNAs, and this difference was diminished in the *dhh1Δ* mutant (Figure 3B, cf. col. 3 versus 1 & 4 versus 2), such that the (C/T) ratio is significantly larger in *dhh1Δ* versus WT cells for the upregulated transcripts (Figure 3C)—all as expected from accumulation of decapped degradation intermediates of the Dhh1-repressed transcripts in WT. The opposite trends were observed for the group of mRNAs down-regulated by *dhh1Δ* (Figures 3B, C); and similar findings were made for the mRNAs dysregulated by *pat1Δ* (Figure S6A–C). These data support the notion that impaired decapping and attendant degradation by Xrn1 is a key contributor to mRNA derepression in *dhh1Δ* and *pat1Δ* cells. Interestingly, analysis of C/T ratios for all iESR mRNAs suggests that their induction in these mutants likewise involves diminished decapping and degradation (Figure S6D, E).

Additional evidence for reduced mRNA decay is provided by published measurements of mRNA turnover rates for a panel of eight mRNAs derepressed in the same mutant strains and growth conditions we employed here (5), which revealed a close correspondence between increased half-lives determined previously and increased mRNA abundance in our RNA-Seq experiments (Figure S7A(i)). We also interrogated published measurements of global mRNA degradation rates determined for WT, *dhh1Δ,* and *pat1Δ* strains that are non-isogenic to those analyzed here (File S8) and found that the groups of mRNAs we identified as significantly up-regulated or down-regulated in abundance by *dhh1Δ* or *pat1Δ* exhibit decreased or increased rates of mRNA decay, respectively, in these mutants (Figure S7A(ii)).

Genes encoding mRNAs derepressed by *dhh1Δ* and *pat1Δ* exhibit reduced RNA polymerase II occupancies in the mutants

To determine whether increased transcription contributes to increased abundance of any mRNAs derepressed by *pat1Δ* or *dhh1Δ*, we performed ChIP-Seq analysis of Rpb1 to measure RNA Polymerase II (Pol II) occupancies averaged across the CDS of every gene, obtaining highly

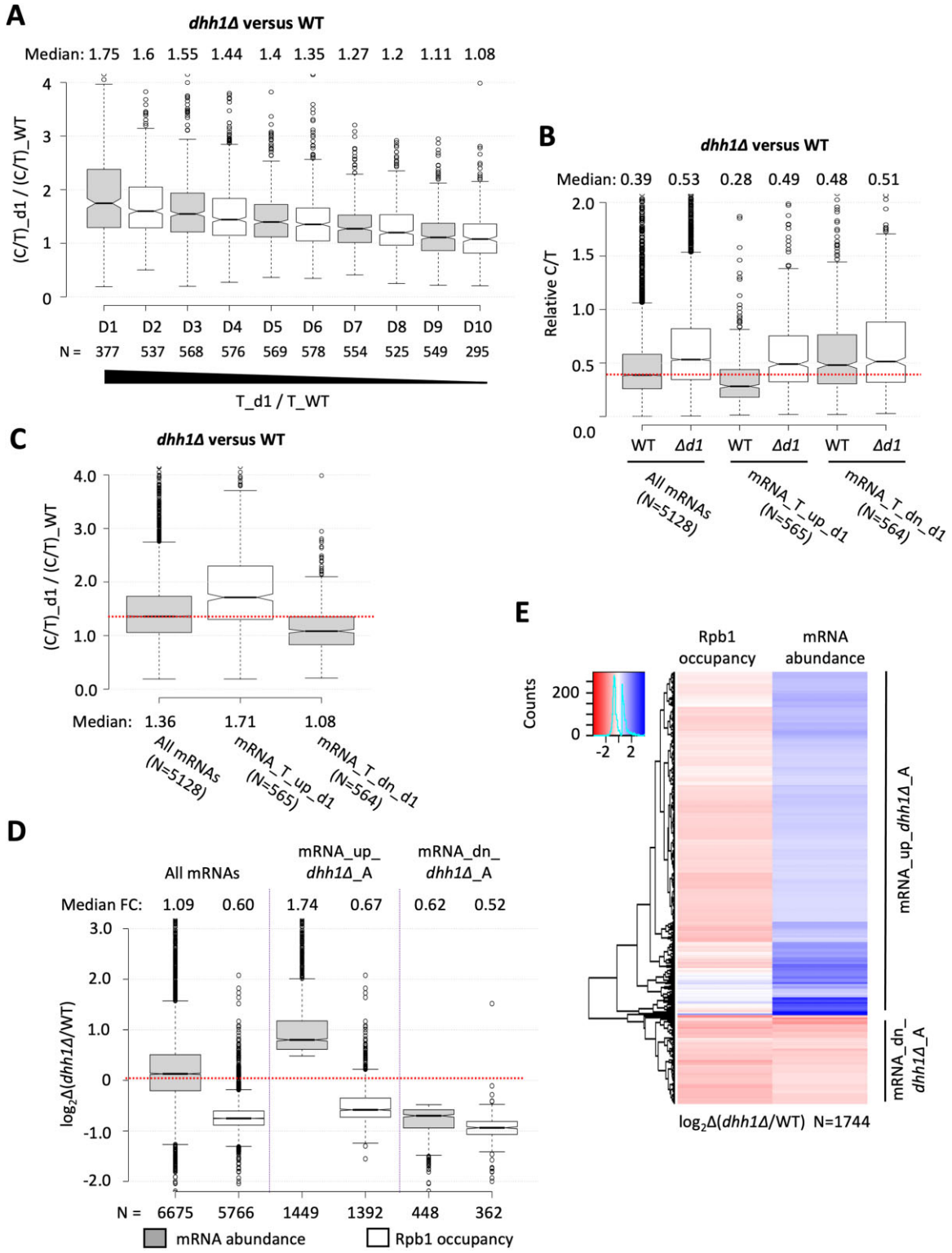

Figure 3. Changes in capped versus total mRNA levels conferred by *dhh1Δ* suggest that decapping is a key driver of changes in mRNA abundance in *dhh1Δ* cells. (**A**) Direct correlation between changes in total mRNA abundance (T) and changes in the ratios of capped to total mRNA abundance in TPMs (C/T) conferred by *dhh1Δ* versus WT. All transcripts were divided among 10 deciles (D1 to D10) based on their changes in total mRNA levels in *dhh1Δ* versus WT (determined by DESeq2 analysis of total RNA reads), ordered from highest to lowest. The change in C/T ratios in *dhh1Δ* versus WT cells was plotted for each decile. **(B, C)** C/T ratios (B) or the changes in C/T ratios in *dhh1Δ* versus WT cells (C) are plotted for either all mRNAs or for the mRNA_T_up_d1 or mRNA_T_dn_d1 groups defined in Table 2. (**D**) Notched box-plot analysis of changes in absolute (spike-in normalized) Rpb1 occupancies or absolute (ERCC-normalized) mRNA abundance in *dhh1Δ* versus WT cells for all mRNAs (cols. 1–2), the 1449 mRNA_up_d1_A transcripts (cols. 3–4), and 448 mRNA_dn_d1_A transcripts (cols. 5–6). (**E**) Hierarchical clustering analysis of the same data from (**D**) (excluding a few outliers with $\log_2\Delta$ values > +4 or < –4).

Table 1. Properties of mRNAs repressed by Dhh1 or Pat1 at the level of mRNA abundance or translational efficiency[a]

(i) mRNA Group	(ii) TE in WT	(iii) CDS length	(iv) 4E/4G occs.	(v) 4E-BP occs.	(vi) stAI	(vii) GO enriched[a]
1. Non-iESR mRNAs w/ abundance repressed by Dhh1[b]	~Avg.	Avg.	>Avg.	>Avg.	~Avg.	Aerobic respiration (TCA cycle and ETC), cell wall and plasma membrane
2. Non-iESR mRNAs w/ abundance repressed by Pat1[c]	>Avg.	<Avg.	>Avg.	<Avg.	~Avg.	Carbohydrate metabolism and aerobic respiration (TCA cycle and ETC), cell wall and plasma membrane
3. mRNAs w/ translation repressed by Dhh1 ($N = 119$)[b]	<<Avg.	>Avg.	>Avg.	>Avg.	Avg.	Cell wall and plasma membrane, cell-cell adhesion
4. mRNAs w/ translation repressed by Pat1 ($N = 271$)[c]	<Avg.	Avg.	>Avg.	~Avg.	>Avg.	Cell wall and plasma membrane, cell-cell adhesion; allantoin utilization; carbon compound metabolism

[a]Determined using FunSpec with P values < 0.05 adjusted by the Bonferroni correction.
[b]Either in WT cells or *pat1Δ* cells; i.e. mRNA_up_d1_c or TE_up-d1_c.
[c]Either in WT cells or *dhh1Δ* cells; ie. mRNA_up_p1_c or TE_up_p1_c.

correlated results between biological replicates for each of the three WT or mutant strains ($r = 0.99$; File S8). To quantify absolute changes in Pol II, *S. pombe* chromatin was added as spike-in to each *S. cerevisiae* chromatin sample prior to immunoprecipitation of Rpb1. To measure absolute changes in mRNA abundance, we analyzed the RNA-Seq data obtained in parallel with CAGE (described above) in which External RNA Controls Consortium (ERCC) transcripts had been spiked-in prior to preparation of cDNA libraries. The spike-in normalized RNA-Seq and Rpb1-ChIP-Seq data sets each showed close correspondence among biological replicates for all strains, as illustrated in Figure S7B.

Considering all mRNAs, the spike-in normalized RNA-Seq data (File S8) revealed significant increases in median total mRNA abundance of 9% or 12% in *dhh1*Δ or *pat1*Δ versus WT, respectively, which was accompanied by decreased median Rpb1 occupancies of 40% in each mutant (Figures 3D & S7C, cols. 1–2). These findings are consistent with a reduced rate of mRNA decay that exceeds reduced transcription across the transcriptome to yield a net increase in total mRNA levels in the mutants. They also fit with results demonstrating that decreased mRNA turnover is buffered by decreased transcription in mutants lacking mRNA degradation enzymes (44). After identifying genes with increased or decreased absolute mRNA abundance between *dhh1Δ* versus WT (> 1.4-fold at FDR < 0.01, mRNA_up_d1_A and mRNA_dn_d1_A), both were found to exhibit decreased Rpb1 occupancies that are merely greater for the mRNA_dn groups (Figures 3D, cols. 3–6). Similar findings emerged for the mRNAs dysregulated by *pat1Δ* (Figure S7C). Cluster analysis confirms that the majority of mRNA_up_A transcripts show reduced absolute Rpb1 occupancies in both mutants versus WT cells (Figures 3E & S7D), indicating that decreased mRNA turnover, not elevated transcription, underlies their derepressed abundance. The fact that most mRNA_dn_A transcripts also show reduced Rpb1 occupancies (Figures 3E & S7D) suggests that their down-regulation actually does involve reduced transcription. Results explained fully in Figure S8 indicate that induction of the group of all iESR transcripts in the mutants also involves diminished decay, but that increased transcription likely contributes to the derepression of the subset known to bind the stress-activated transcriptional activator Msn2 (45).

The mRNAs most strongly repressed by Dhh1 or Pat1 are not poorly translated or enriched for suboptimal codons

In view of evidence that competition between translation initiation factors and mRNA degradation enzymes determines mRNA turnover (1), we asked whether mRNAs targeted by Dhh1 or Pat1 for degradation are poorly translated in WT cells. To the contrary, examining the translational efficiencies (TEs) of mRNAs by ribosome profiling (presented below) showed that the mRNA_up_p1_c transcripts derepressed by *pat1Δ* exhibit a ~1.25-fold greater TE in WT cells compared to all mRNAs (Figure S9A, col. 1). In agreement with the inverse relationship between TE and CDS length (46), the mRNAs derepressed by *pat1Δ* also have a shorter CDS length compared to those repressed in the mutant versus WT (Figure S9B) (File S5). Moreover, based on published RIP-seq data (47) (File S5), the derepressed mRNAs have greater than average occupancies of cap-binding initiation factors eIF4E and eIF4G and poly(A)-binding protein Pab1, but lower occupancies of inhibitory eIF4E-binding proteins Caf20 and Eaf1 (Figure S9C(i)). The findings that Pat1-repressed mRNAs tend to be well-translated and enriched for the factors that mediate closed-loop initiation intermediates (summarized in Table 1) seem at odds with the possibility that poorly translated mRNAs are preferentially targeted for degradation by Pat1. Although the Dhh1-repressed mRNAs exhibit enrichment for eIF4E-binding proteins as well as eIF4E/eIF4G1 (Figure S9C(ii)), their average median TE in WT (Figure S9A, col. 2) does not support the possibility that Dhh1 targets poorly initiated mRNAs (Table 1).

Dhh1 functions in the mechanism that targets mRNAs enriched with suboptimal codons for enhanced degradation (19). Previously, codon nonoptimality was linked with Dhh1-mediated mRNA decay in part by demonstrating an inverse correlation between stAI values, a measure of overall codon optimality of mRNA (48) (tabulated in File S5), and the change in mRNA abundance in *dhh1Δ* versus WT cells (19), which we had also observed in our RNA-Seq data on *dhh1Δ* (23). However, the median stAI values of the

Table 2. Different transcript groups identified by RNA-Seq analysis done in parallel with Ribo-Seq or CAGE-Seq analysis of the three mutants versus WT analyzed in this study[a]

Groups	*pat1Δ*	*dhh1Δ*	*pat1Δdhh1Δ*
Dhh1- or Pat1-regulated transcripts identified by RNA-Seq in parallel with Ribo-Seq	mRNA_up_p1 (747)	mRNA_up_d1 (592)	mRNA_up_p1d1 (982)
	mRNA_dn_p1 (600)	mRNA_dn_d1 (545)	mRNA_dn_d1 (1052)
Dhh1- or Pat1-regulated non-ESR transcripts identified by RNA-Seq in parallel with Ribo-Seq	non-iESR_mRNA_up_p1 (590)	non-iESR_mRNA_up_d1 (431)	non-iESR_mRNA_up_p1d1 (774)
	non-iESR_mRNA_dn_p1 (480)	non-iESR_mRNA_dn_d1 (363)	non-iESR_mRNA_dn_d1 (826)
Combined groups of Dhh1- or Pat1-repressed non-ESR transcripts identified by RNA-Seq in parallel with Ribo-Seq	mRNA_up_p1_c (835)	mRNA_up_d1_c (609)	
	mRNA_down_p1_c (676)	mRNA_down_d1_c (578)	
Dhh1- or Pat1-regulated capped transcripts identified by CAGE-Seq	mRNA_C_up_d1 (1321)	mRNA_C_up_d1 (1185)	
Dhh1- or Pat1-regulated total transcripts (capped and uncapped) identified by RNA-Seq in parallel with CAGE-Seq	mRNA_T_up_p1 (1022)	mRNA_T_up_d1(767)	
	mRNA_T_dn_p1 (712)	mRNA_T_dn_d1 (836)	
Dhh1- or Pat1-regulated transcripts identified by ERRC-normalized RNA-Seq in parallel with CAGE-Seq	mRNA_up_p1_A (1401)	mRNA_up_d1_A (1449)	
	mRNA_dn_p1_A (424)	mRNA_dn_d1_A (449)	

[a]Number of transcripts in each group is listed in parenthesis.

mRNAs derepressed by *pat1Δ* or *dhh1Δ* are virtually indistinguishable from that for all mRNAs (Figure S9D). This finding suggests that one or more other transcript features are more important than codon non-optimality in targeting mRNAs for degradation by Pat1 or Dhh1 (Table 1).

Pat1 and Dhh1 functionally cooperate to control the translation of particular mRNAs

We sought next to elucidate the roles of Pat1 and Dhh1 in controlling the translation of individual mRNAs. DESeq2 analysis of our Ribo-Seq data identified 144, 51 and 244 mRNAs showing relative TE increases of > 1.41-fold at FDR < 0.10 in the *pat1Δ, dhh1Δ* or *pat1Δdhh1Δ* mutant compared to WT, respectively (File S10). These groups of mRNAs, designated TE_up_d1, TE_up_p1 and TE_up_p1,d1, overlapped extensively (Figure 4A), and the mRNAs translationally derepressed in all three mutants exhibit strong TE increases of similar magnitude in all three mutants (Figure 4C(v)), as illustrated for *SSA3* mRNA (Figure 4B). Thus, both Dhh1 and Pat1 are required for appreciable repression of these transcripts, indicating interdependent functions. At the other extreme, mRNAs exhibiting marked TE increases only in the double mutant show a cumulative effect of the two mutations (Figure 4C (vii)), indicating that each factor exerts translational repression in the absence of the other. DESeq2 analysis of the TE increases conferred by *pat1Δ* on comparing the *pat1Δdhh1Δ* double mutant to the *dhh1Δ* strain identified additional mRNAs translationally repressed by Pat1 only in cells lacking Dhh1, to yield a combined group of 273 Pat1-repressed mRNAs (TE_up_p1_c; Figure S10A (File S11). Similarly, we identified a more comprehensive group of 121 mRNAs translationally repressed by Dhh1 (TE_up_d1_c; Figure S10B). Cluster analysis reveals similar TE changes in all three mutants for many transcripts in both combined groups (Figure S10C, D), as exemplified for most of the 61 mRNAs common to both sets, indicating interdependent repression by Dhh1 and Pat1 (Figures 4D(iii), E). These last mRNAs are distinctive in being very poorly translated in WT cells (Figure 4F(iii)) and in showing Pat1 repression of mRNA abundance as well (Figure S10E(iii)). Their low TEs are not, however, associated with lower than average stAI values (0.36 versus 0.35 for all mRNAs), nor with atypically low occupancies of eIF4F or Pab1 or high occupancies of inhibitory eIF4E-binding proteins (Figure S10F(iii)). As such, it is possible that recruitment of Pat1 and Dhh1 to these transcripts by RNA binding proteins underlies their pronounced translational repression.

To validate translation changes in the mutants, we conducted proteomics using TMT mass spectrometry (MS) of total protein isolated from the *dhh1Δ, pat1Δ, pat1Δdhh1Δ* and WT strains, obtaining data for > 4000 proteins that was highly correlated among three biological replicates for each strain (Pearson $r > 0.99$) (File S12). Importantly, we observed significant correlations between changes in protein and RPF abundance across all proteins for all three mutants (Figure 5A–C); and found that groups of mRNAs exhibiting increased or decreased RPFs in the mutants (> 1.5-fold, FDR < 0.05) showed corresponding increases or decreases in protein abundance by TMT-MS/MS (Figure 5D). Considering that differential protein degradation rates can alter steady-state protein levels, the significant correlations observed here between ΔRPFs and Δprotein levels suggest an even greater correspondence between RPF abundance and protein synthesis rates for most mRNAs. The groups of 51 and 144 mRNAs showing

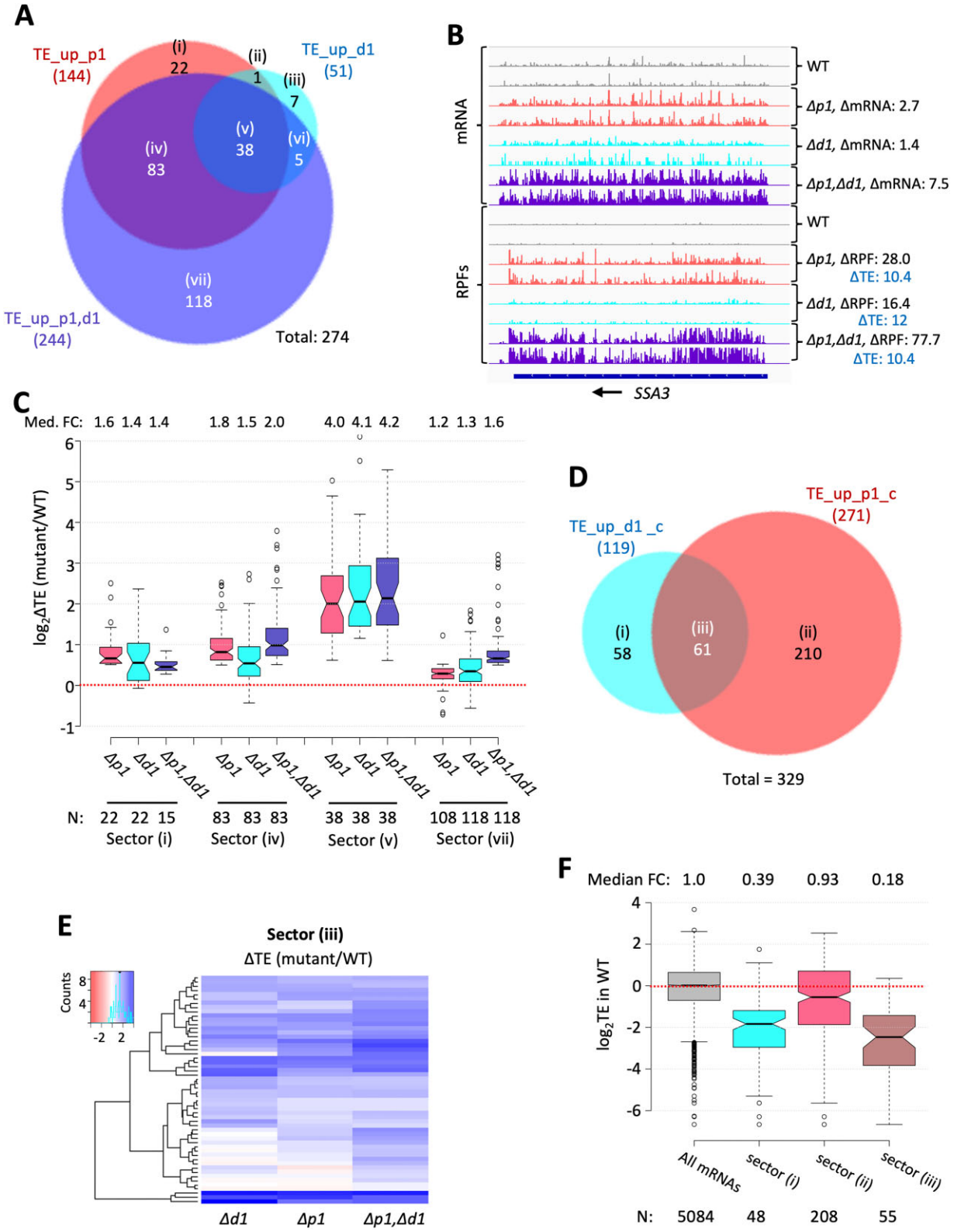

Figure 4. Extensive cooperation between Pat1 and Dhh1 in repressing the translation of many mRNAs, ranging from functional redundancy to interdependence. (**A**) Venn diagram showing the overlap between the three groups of mRNAs whose TEs are derepressed by the *pat1Δ*, *dhh1Δ* or *pat1Δdhh1Δ* mutations versus WT. (**B**) Gene browser image for *SSA3* presented as in Figure 1A. (**C**) TE changes conferred by the same three mutations are plotted for the mRNAs belonging to the indicated sectors of the Venn diagram in (A). (**D**) Venn diagram showing the overlap between the group of 271 mRNAs that belong uniquely to the TE_up_p1_c group and the 119 mRNAs that belong uniquely to the TE_up_d1_c group, defined in Figure S10A and B. (**E**) Hierarchical clustering analysis of $\log_2\Delta$TE values conferred by the indicated mutations versus WT for 54 of the 61 mRNAs from sector (iii) in (D). (**F**) $\log_2$TE in WT cells for all mRNAs and the mRNAs in the three sectors from (D).

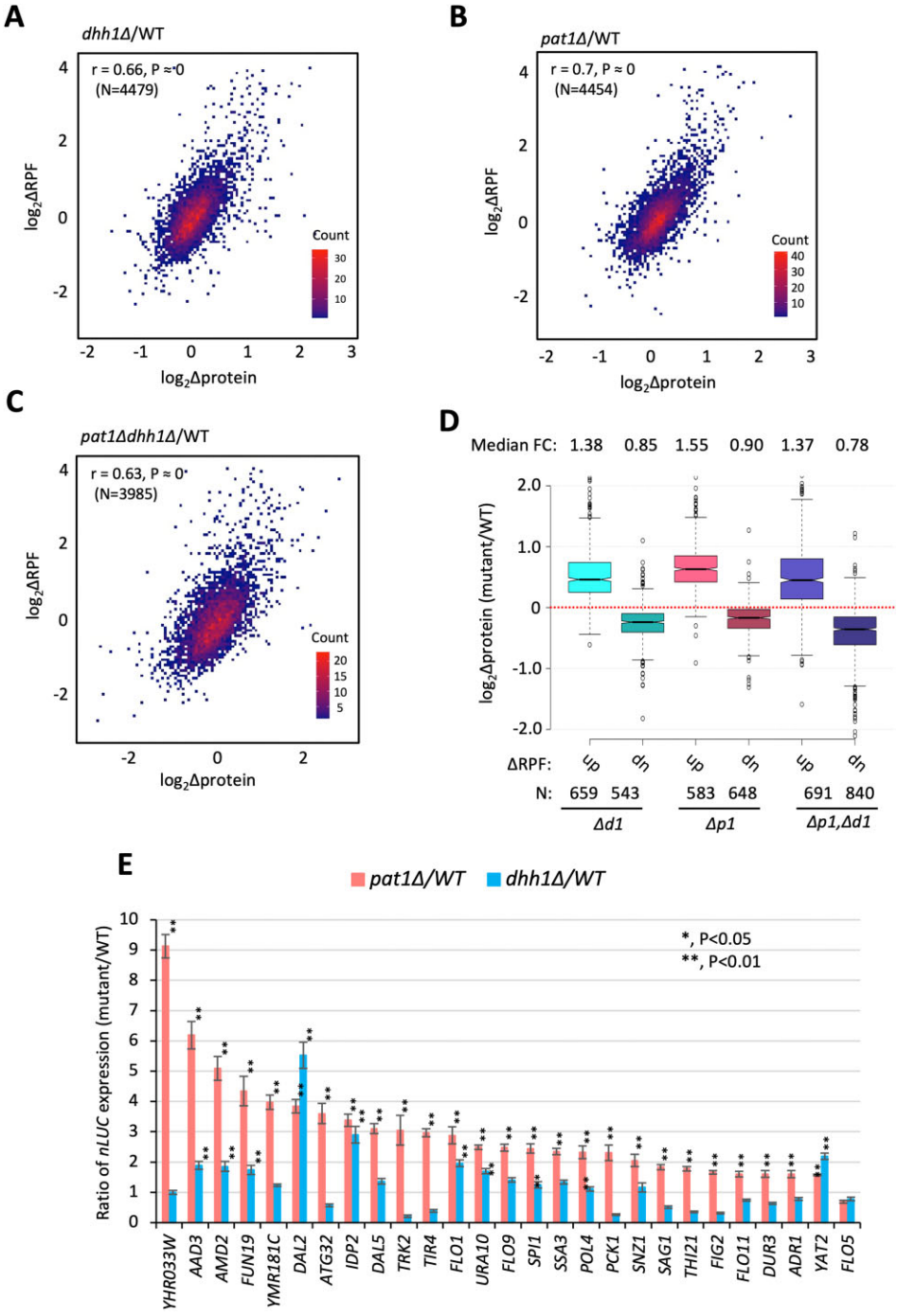

Figure 5. Changes in protein expression measured by TMT-MS/MS are correlated with changes in RPF abundance in the *pat1Δ*, *dhh1Δ* and *pat1Δdhh1Δ* mutants. (**A–C**) Density-scatterplots of changes in RPFs measured by ribosome profiling versus changes in protein expression determined by TMT-MS/MS for all proteins detected in the latter experiment (*N*), with Pearson coefficients and *P* values indicated for the correlation analyses. (**D**) Protein changes from TMT-MS/MS conferred by the indicated mutations versus WT for the groups of mRNAs showing > 1.5-fold increases in RPFs at FDR < 0.05 in response to the corresponding mutations versus WT. (**E**) Expression of *nLUC* reporters in *pat1Δ* or *dhh1Δ* mutants relative to WT for the indicated genes. Luciferase activity was measured in cell extracts and normalized to total protein for at least three independent transformants for each reporter in cells grown in synthetic complete medium lacking uracil to A_{260} of 1.0–1.5. Mean values ± S.E.M. are plotted. Results of t-tests of the differences in mean expression between mutant and WT are indicated as: **P* < 0.05, ***P* < 0.01.

elevated TEs in *dhh1Δ* and *pat1Δ* cells also exhibit significantly increased protein abundance, by factors of 1.82 and 1.65, respectively. This last finding of increased RPF density (TE) associated with increased protein expression in the mutants is consistent with Dhh1/Pat1 repressing mRNA translation by inhibiting initiation versus elongation.

To provide additional support for increased translation of a subset of the 61 mRNAs described above displaying strong translational repression by Pat1 and Dhh1, we assayed reporters with nanoLUC CDSs inserted before the stop codons. We observed increased expression of all but one of the 27 reporters in *pat1Δ* versus WT cells (Figure 5E) (File S12), supporting repression of the corresponding native genes by Pat1. Only 1/3rd of the reporters also showed increased expression in *dhh1Δ* versus WT cells (Figure 5E), however, even though the genes for seven of the non-derepressed reporters (*YHR033W, DAL5*, *SSA3, PCK1, SNZ1, THI21* and *ADR1*) showed increased protein expression in *dhh1Δ* cells by TMT-MS/MS. Perhaps translational repression by Dhh1 is easily perturbed by alterations of mRNA structure resulting from *nLUC* insertion.

Post-transcriptional repression by Pat1 and Dhh1 of genes required for respiration or catabolism of non-preferred carbon or nitrogen sources

We conducted gene ontology (GO) analysis to assess whether mRNAs targeted by Dhh1 or Pat1 for either degradation or translational repression are involved in the same cellular functions. In addition to the iESR stress response mRNAs induced in both mutants (Figure 1B–D), the non-iESR mRNAs up-regulated by *pat1Δ* are enriched for genes involved in carbohydrate metabolism or respiration, including the tricarboxylic acid (TCA) cycle and electron transport chain (ETC), and for proteins localized to membranes, the cell wall, or in mitochondria (adjusted P-value < 0.05; Table 1). The non-iESR mRNAs derepressed by *dhh1Δ* are likewise enriched for genes involved in respiration or localized to membranes or cell wall (Table 1) (File S9). The mRNAs translationally repressed by Pat1 (TE_up_p1_c) are also enriched for cell wall and plasma membrane proteins, including cell adhesion proteins (agglutinins), proteins involved in utilizing non-preferred nitrogen source allantoin, or in carbon metabolism (Table 1). The mRNAs translationally repressed by Dhh1 (TE_up_d1_c) are likewise enriched for agglutinins (Table 1) and include allantoin catabolic genes *DAL5* (illustrated in Figure S11A) and *DAL2*. Examining a group of 61 cell wall or agglutinin mRNAs up-regulated in abundance or TE by *pat1Δ* or *dhh1Δ* revealed that derepression generally occurs at the mRNA level, with small TE increases limited to the *pat1Δdhh1Δ* double mutant (Figure S11B); although TE increases are prominent for the agglutinins (Figure S11C).

Interrogating a group of 51 nucleus-encoded transcripts directly involved in mitochondrial oxidative phosphorylation (Ox. Phos.), required for energy generation from non-fermentable carbon sources, shows depression in the three mutants primarily at the level of mRNA abundance (Figure 6A). Western blot analysis confirmed increased expression of four Ox. Phos. proteins (Qcr8, Atp20, Idh1 and Sdh4), two proteins involved in cytochrome c oxidase assembly (Cox14 and Cox20), and cytochrome b2 (Cyb2, mitochondrial protein required for lactate utilization) in the *dhh1Δ* and *pat1Δdhh1Δ* strains, which (except for Cyb2 and Atp20) also occurred in *pat1Δ* cells (Figures 6B-C). Derepression in the three mutants also occurred for transcripts encoding enzymes of the glyoxylate cycle (Figure S11D), which catalyze reactions of the TCA cycle outside of mitochondria to support gluconeogenesis during respiratory growth on two-carbon compounds; and increased expression of one such enzyme encoded by *CIT2* was confirmed for *dhh1Δ* cells by western blot analysis (Figures 6B, C).

We obtained independent support that eliminating Dhh1 or Pat1 elevates respiration during growth on glucose by measuring mitochondrial membrane potential ($\Delta\Psi_m$) produced by the ETC using the probe tetramethylrhodamine (TMRM)—a cationic fluorescent dye that accumulates in mitochondria as a function of $\Delta\Psi_m$. Quantifying dye fluorescence by flow cytometry revealed increased TMRM fluorescence in the *dhh1Δ* and *pat1Δ* strains containing empty vectors compared to both the WT strain and the mutant strains complemented by the WT genes (Figure 6D) (File S13). Thus, increased expression of Ox. Phos. genes in the mutants is sufficient to elevate mitochondrial ETC activity in glucose-grown cells.

Related to the derepression of Ox. Phos. genes, a group of 83 carbon catabolite repressed (CCR) mRNAs (File S13) known to be glucose-repressed or activated by transcription factors Adr1 or Cat8 (49,50), exhibit increased median levels of translation (RPFs) driven largely by increased mRNA abundance in all three mutants (Figure S12A). Interestingly, *ADR1* expression is derepressed in all three mutants (ΔRPFs of 4.2- to 19-fold); however, activation of Adr1 function by Snf1 kinase is not expected in high-glucose YPD medium (51). We analyzed Adr1 function in the mutants by assaying an *ADH2-lacZ* reporter known to be transcriptionally induced by activated Adr1 (52). As expected, *ADH2-lacZ* expression was ∼100-fold higher in WT cells grown with glycerol/ethanol versus glucose as carbon source (Figure S12B(i)). Importantly, however, *ADH2-lacZ* expression was reduced in all three mutants versus WT cells on glucose medium (Figure 12B(ii)). Consistent with this, the CCR genes exhibit reduced Rpb1 occupancies, indicating decreased transcription rates, in both *dhh1Δ* and *pat1Δ* cells versus WT (Figure S12E(i)). These findings imply that CCR transcripts are derepressed in the mutants owing to reduced mRNA degradation rather than increased transcriptional activation.

In similar experiments, we obtained evidence that transcription factors responsible for induction of Ox. Phos. genes, the Hap2/Hap3/Hap4/Hap5 complex, are not activated in our mutants. Thus, a Hap complex-activated *CYC1-lacZ* reporter (53), which showed the expected induction in WT cells grown with glycerol/ethanol versus glucose (Figure 6E(i)) (51), was only slightly derepressed in *dhh1Δ* cells and repressed in *pat1Δ* and *pat1Δdhh1Δ* mutants grown on glucose (Figure 6E(ii)). Moreover, the Rpb1 occupancies of Ox. Phos. genes were reduced in the *dhh1Δ* and *pat1Δ* strains (Figure S12E(ii)), implying that increased expression of Ox. Phos. transcripts results from reduced mRNA turnover.

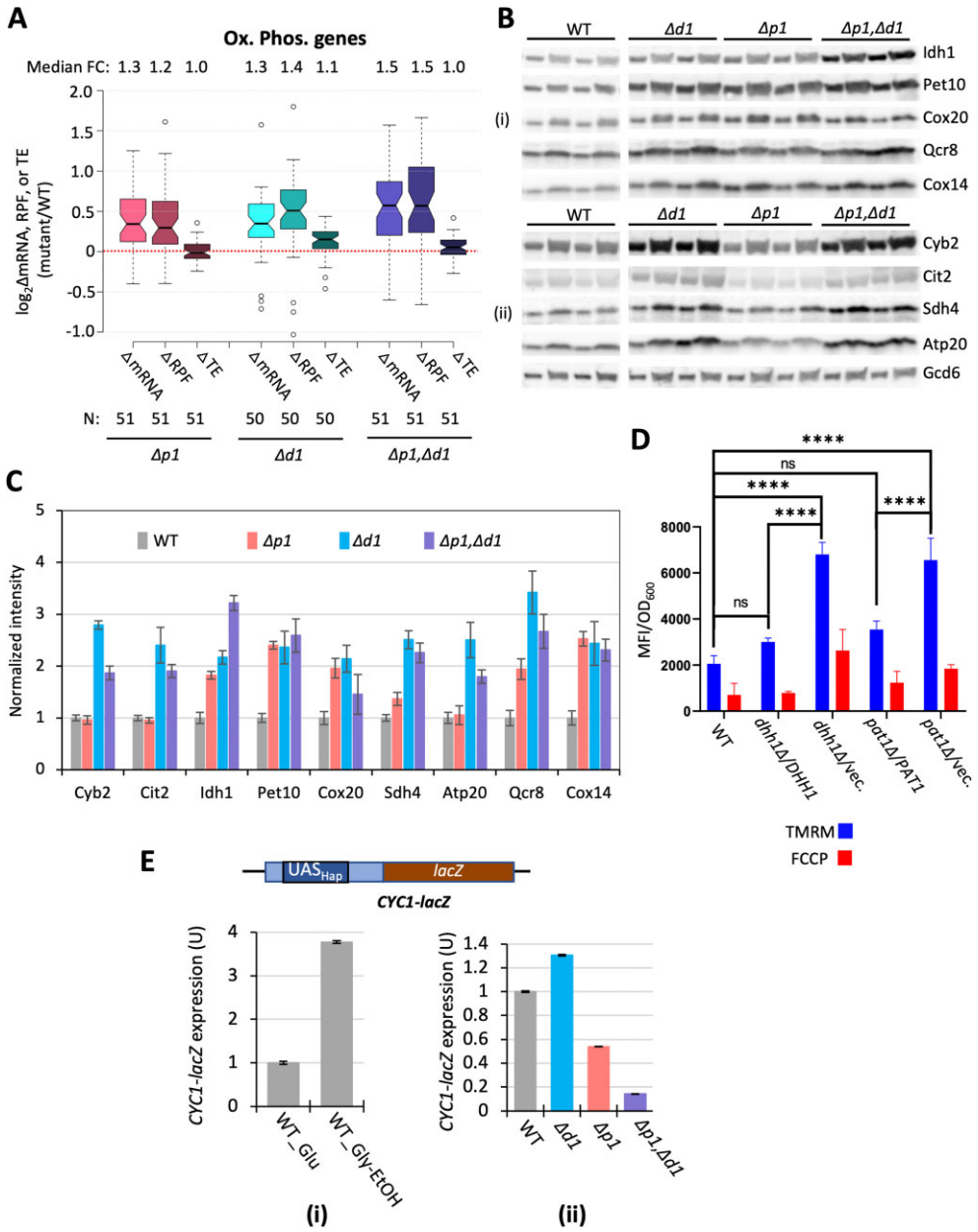

Figure 6. Pat1 and Dhh1 repress the abundance of mRNAs involved in respiration and suppress mitochondrial membrane potential in rich medium. (**A**) Changes in mRNA, RPFs, or TE conferred by the indicated mutations versus WT for 51 genes encoding mitochondrial proteins involved directly in oxidative phosphorylation. (**B, C**) Western blot analysis of 9 mitochondrial proteins and Gcd6 (examined as loading control) in the WT and indicated mutant strains, cultured in duplicate in YPD medium to A_{600} of ∼0.6–0.8. WCEs were extracted under denaturing conditions and aliquots corresponding to 1× or 2× amounts of WCE were loaded in successive lanes for the two replicate cultures. Immune complexes were visualized with enhanced chemiluminescence (B). Signals for each protein were quantified, normalized to the corresponding signals for Gcd6 in the same extract, and expressed relative to the resulting values for WT cells. Mean values and standard errors are plotted (C). (**D**) WT or transformants of the *dhh1Δ* or *pat1Δ* strains containing empty vector or plasmids bearing *DHH1* (pJI277) or *PAT1* (pNG162), respectively, were cultured in SC-Ura to mid-log phase. TMRM (500 nM) was added and incubated for 30 min before samples were collected and washed once with deionized water. $\Delta\Psi_m$ was determined by measuring TMRM fluorescence intensity using flow cytometry. Data are presented in arbitrary fluorescence intensity units per OD_{600}. Two-way ANOVA was used for statistical analysis and data are given as mean values ± SD ($n = 3$) (****$P < 0.0001$). (**E**) Expression of the *CYC1-lacZ* reporter on plasmid pLG265, lacking UAS1 and containing the optimized version of UAS2, UAS2UP1, in the WT strain grown on SC-Ura medium containing either 2% glucose or 3% glycerol/2% ethanol as carbon sources (i), or in WT and the indicated mutant strains on SC-Ura with 2% glucose (ii). β-Galactosidase activity (nmoles of o-nitrophenyl-β-D-galactopyranoside (ONPG) cleaved per min per mg of total protein) was measured in whole cell extracts for three biological replicates of each strain and the mean values were normalized to the mean activity measured in WT grown with glucose as carbon source.

The allantoin degradation genes derepressed in the mutants are among a larger group of nitrogen catabolite repressed (NCR) genes, transcriptionally repressed by preferred nitrogen sources (54). Notably, the group of all such NCR genes (File S13) is derepressed in the *pat1Δ, dhh1Δ,* and *pat1Δdhh1Δ* mutants at the level of mRNA abundance (Figure S12C). However, the key transcriptional activators of these genes, Gln3 and Gat1, appear to be less functional in the mutants, judging by reduced expression of a modified *CYC1-lacZ* reporter driven by Gln3/Gat1 GATA binding sites in the presence of preferred nitrogen source ammonium sulfate (Figure S12D(ii)). This reporter exhibits the expected strong induction in WT cells cultured with proline versus ammonium sulfate (51) (Figure S12D(i)) (File S14 contains all *lacZ* reporter data). These findings, combined with the reduced Rpb1 occupancies of the NCR genes in *dhh1Δ* and *pat1Δ* mutants (Figure S12E(iii)), indicates that derepression of NCR transcripts in the mutants involves reduced degradation versus increased transcription.

In summary, numerous genes involved in respiration, utilization of non-preferred carbon or nitrogen sources, or cell adhesion are derepressed post-transcriptionally in the *pat1Δ, dhh1Δ,* and *pat1Δdhh1Δ* mutants.

Pat1 cooperates with Dhh1 to suppress autophagy in non-starvation conditions

Previously, evidence was presented that a subset of mRNAs whose products function in autophagy are targeted for enhanced decapping and degradation by Dhh1, which helps to suppress autophagy in nutrient-rich conditions (9). Our data support these findings and expand the group of Dhh1-repressed genes from *ATG3,-7,-8, -19, -20, -22* and *-24* to include *ATG1,* a key protein kinase regulator of the pathway, as well as *ATG9, -4, -2* and *-21.* While not acting as broadly, we found that Pat1 also contributes to repressing autophagy genes *ATG8, -19, -22, -3, -4, -23* and *-24*. These changes are almost entirely at the mRNA level (Figure 7A). Pat1 was previously implicated in promoting, rather than preventing, autophagy during nitrogen starvation, by impeding degradation of *ATG1, -2, -7* and *-9* mRNAs (10). None of these last *ATG* mRNAs were derepressed here by *pat1Δ* in rich medium, suggesting that Pat1 oppositely regulates distinct *ATG* transcripts to help repress autophagy in nutrient-replete cells while activating the process in starved cells.

ATG8 is the most strongly induced autophagy gene in starved cells (55) and also the most highly derepressed in the mutants studied here (Figure 7B). Elevated Atg8 is associated with larger autophagosomes and increased autophagy. Examining expression of a GFP-Atg8 fusion protein confirmed derepression of *ATG8* in the mutants, which was most pronounced for *pat1Δ* (Figure 7C). This construct also provides a reporter for autophagic flux, as Atg8 trapped in autophagosomes is degraded after their fusion with vacuoles, but the cleaved GFP moiety accumulates (10). No free GFP was detected in WT cells cultured on YPD where autophagy is suppressed, whereas free GFP was detected in all three mutants, with greatest accumulation in *pat1Δdhh1Δ* cells (Figures 7C, D) (File S15). While increased expression of Atg8 in *dhh1Δ* cells has been reported, increased autophagy on rich medium was not detected previously in *dhh1Δ* (9) or *pat1Δ* mutants (10). Thus, in our strain background, derepression of multiple *ATG* mRNAs on loss of Dhh1 or Pat1 is sufficient to confer autophagy inappropriately on rich medium in a manner exacerbated by simultaneous loss of both proteins.

DISCUSSION

By conducting ribosome profiling and RNA-Seq on mutants lacking Pat1, Dhh1, or both proteins, we identified groups of mRNAs that appear to be targeted for enhanced degradation or translational repression by these factors in cells grown in nutrient-rich medium with preferred carbon source glucose. Although the ESR is mobilized, it does not account for 73–80% of the transcripts up-regulated in *pat1Δ* or *dhh1Δ* cells. Because the ESR is likely a response to the slow-growth phenotypes of the mutants (39), we removed iESR mRNAs from consideration to focus on the transcripts most likely to be targeted directly by Pat1 and Dhh1 for degradation in non-stressed cells.

Previous work suggested that, despite considerable overlaps between the mRNAs repressed by Dhh1 or Pat1, ∼50% were repressed exclusively by one or the other factor (5). While a similar conclusion is suggested by the gene overlap analysis in Figure 1E, examining the degree of mRNA changes for different subsets in Figure 1F revealed that ∼3/4th of all transcripts derepressed in *pat1Δ, dhh1Δ* or *pat1Δdhh1Δ* cells show increased abundance in both single mutants. Of these 782 transcripts, ∼56% show a comparable increase in the two single mutants while the remaining ∼44% show greater depression in one single mutant versus the other; however, mRNAs of both groups generally display relatively greater derepression in the double mutant. Only the remaining ∼25% of all 1018 derepressed transcripts were up-regulated exclusively in one of the two single mutants with no evidence of greater derepression in the double mutant. We conclude that independent cumulative contributions by Pat1 and Dhh1 represents their predominant mode of functional interaction in repressing mRNA abundance. By examining the *pat1Δdhh1Δ* double mutant we identified many transcripts derepressed only when both factors were missing, thus exhibiting largely redundant contributions of Pat1 and Dhh1 in repressing mRNA abundance. This discovery of mRNAs derepressed by *pat1Δ* only in cells lacking Dhh1 is consistent with the recent finding that binding of Pat1 to the Dcp2 CTT was required for degradation of certain Dhh1-targeted mRNAs only when Dhh1 recruitment to the CTT was compromised (4).

A simple way to explain the cumulative contributions of Pat1 and Dhh1 in repressing mRNA abundance is to propose that they independently activate decapping by Dcp1/Dcp2. Supporting this idea, our RNA-Seq data on the isogenic *dcp2Δ* mutant (23) indicates that the mRNAs derepressed by *dhh1Δ* or *pat1Δ* are enriched for mRNAs showing comparable derepression in cells lacking Dcp2. Moreover, we found that deleting *DHH1* in *dcp2Δ* cells had little effect on the abundance of transcripts derepressed in the *dhh1Δ* single mutant, as expected if Dhh1 represses mRNAs primarily by activating decapping. Furthermore, comparing capped mRNA abundance measured by CAGE and

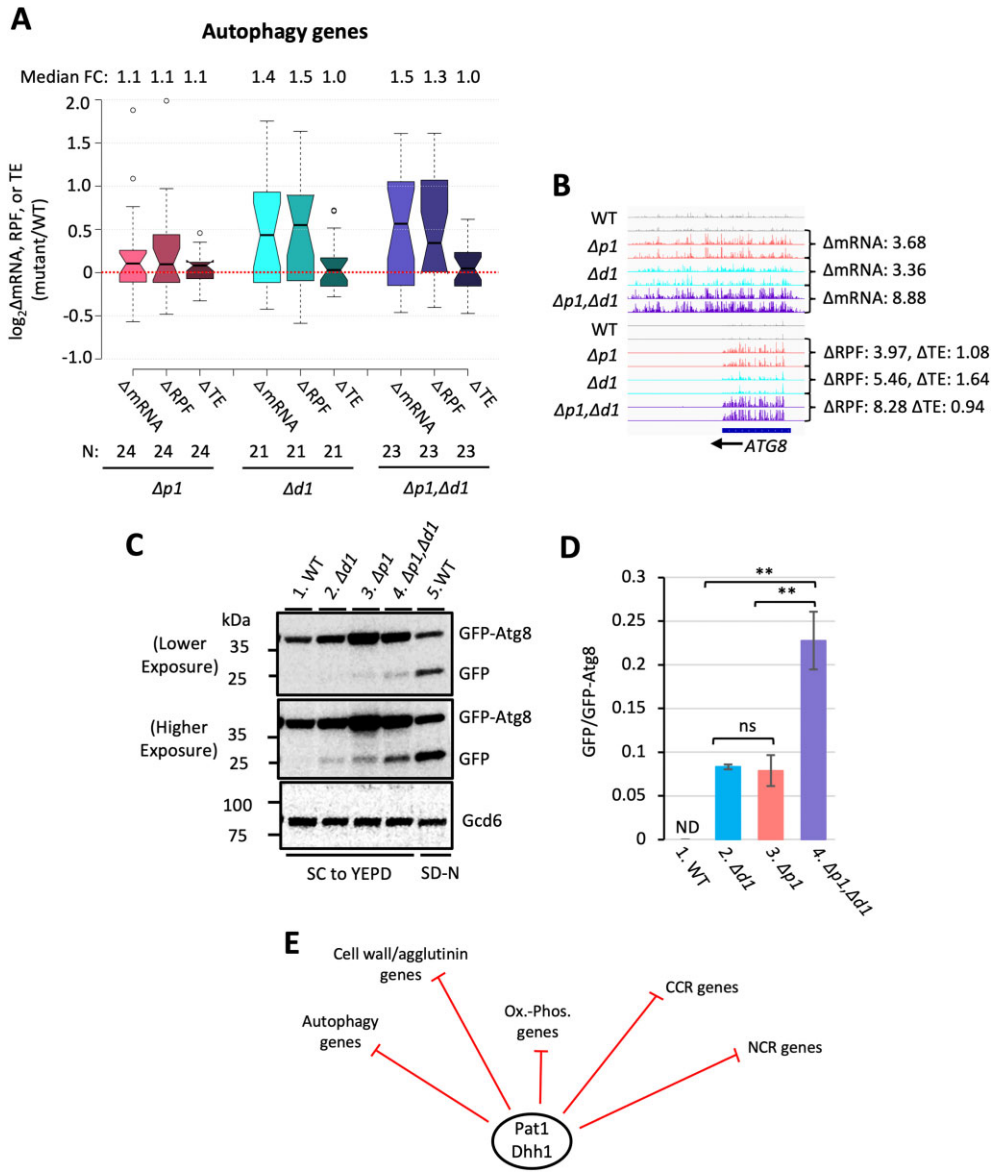

Figure 7. Pat1 and Dhh1 repress the abundance of mRNAs involved in autophagy on nutrient-rich medium. (**A**) Changes in mRNA, RPFs, or TE conferred by the indicated mutations versus WT for 24 genes involved directly in autophagy. (**B**) Gene browser images for *ATG8* showing the mRNA reads (top 8 tracks) and RPF reads (bottom 8 tracks) as shown in Figure 1A. (**C, D**) Autophagy was measured by GFP-Atg8 processing in WT and mutant strains containing plasmid pRS416GFP-ATG8 encoding the GFP-Atg8 fusion protein. Strains were pre-cultured in SC-Ura to maintain the plasmid and transferred to YPD medium for one cell-doubling. Cell extracts were prepared under denaturing conditions and probed with antibodies against GFP or Gcd6, and a representative image is shown (C). The GFP:GFP-Atg8 ratio was quantified from results obtained from two independent cultures, with replicate western blots prepared for each culture, and mean values ± S.E.M. are plotted for $N = 4$ (**D**). Results of *t*-tests are indicated as: $*P < 0.05$, $**P < 0.01$. (**E**) Summary of gene groups or cellular pathways post-transcriptionally down-regulated by Pat1 and Dhh1 in nutrient-replete cells (see text for details).

total mRNA abundance by RNA-Seq revealed that mRNAs derepressed in *dhh1Δ* or *pat1Δ* cells tend to have lower than average proportions of capped transcripts in WT cells, but not in the respective *dhh1Δ* or *pat1Δ* mutants, in the manner expected if mRNAs are frequently repressed by Dhh1 or Pat1 by enhancing decapping and attendant decay. This inference is supported by our Pol II ChIP-Seq data indicating that most genes encoding mRNAs derepressed in the mutants exhibit lower, not higher, Pol II occupancies in *dhh1Δ* and *pat1Δ* cells. Indeed, we observed a global reduction in Pol II occupancies in these mutants in the manner expected from transcriptional buffering of impaired mRNA decay (44). Our conclusion that Pat1 and Dhh1 independently activate decapping of many mRNAs is consistent with the previous identification of distinct segments of the Dcp2 CTT that mediate independent recruitment of Dhh1 (via Edc3/Scd6) or Pat1, and with evidence for distinct decapping complexes containing only Dhh1 or Pat1 (4). We noted previously that Dhh1 occupancy, as determined by RIP-Seq analysis (56), tends to be elevated for mRNAs derepressed by *dhh1Δ* (23), as expected if Dhh1 directly targets mRNAs for decapping/decay. Interestingly,

here we observed elevated Dhh1 association for mRNAs derepressed by *pat1Δ* as well (Figure S13A) (File S16), consistent with Dhh1 contributing to the decay of mRNAs targeted by Pat1.

It is interesting that a subset of the transcripts derepressed by *dhh1Δ* or *pat1Δ* are not equally elevated by *dcp2Δ* (Figure 2C), raising the possibility that certain mRNAs are targeted by Dhh1 or Pat1 for 3′ to 5′ degradation by the cytoplasmic exosome. It is also noteworthy that many mRNAs derepressed in the *dcp2Δ* mutant are not similarly derepressed by *dhh1Δ* or *pat1Δ* (Figure 2C), suggesting that they might be more dependent on other decapping activators. Indeed, we recently presented evidence that a large fraction of the mRNAs targeted for degradation by Dcp2 rely on the Upf proteins, responsible for nonsense-mediated mRNA decay (NMD), rather than on Dhh1, Pat1, Edc3 or Scd6 for their enhanced decapping/degradation (Vijjamarri et al. bioRxiv 2023.01.05.522830).

The mRNAs whose abundance is repressed by Pat1 tend to be efficiently translated in WT cells, enriched for initiation factors eIF4F and Pab1, and depleted of inhibitory eIF4E binding proteins (Table 1), which seems inconsistent with Pat1 enhancing their decapping owing to reduced competition with initiation factors for accessibility to the mRNA cap. The latter mechanism is more plausible for the mRNAs repressed by Dhh1 based on their enrichment for eIF4E-BPs. Neither group of mRNAs displays enrichment for non-optimal codons, however, suggesting that ribosome pausing at non-optimal codons during elongation is not a major determinant of the Dhh1 or Pat1-enhanced degradation of these highly repressed transcripts; although, a stretch of poor codons could still serve as an important trigger for their decay.

Our finding that mRNAs whose abundance is repressed by Pat1 exhibit greater than average TEs (Figure S9A) differs from that of He *et al*. (2018), who concluded that they have low rates of translation elongation, based on low codon optimality and steady-state protein levels but relatively high RPFs (5). As noted above, the Pat1-repressed mRNAs identified here exhibit average codon optimality scores (Figure S9D, col. 2). While our TMT-MS/MS data does indicate low protein abundance in WT for these transcripts (Figure S13B, col. 2), this may arise from low mRNA abundance rather than poor translation (Figure S13C, col. 2), because they have elevated ratios of protein to mRNA levels (Figure S13D, col. 2). The same arguments apply to the mRNAs repressed in abundance by Dhh1 (Figure S13B-D).

By ribosome profiling we identified sets of mRNAs that appear to be repressed at the translational level by Pat1, Dhh1, or both factors. While ribosome profiling of *dhh1Δ* cells has been conducted previously, our analyses of the *pat1Δ* and *pat1Δdhh1Δ* mutants allowed a more comprehensive identification of Dhh1 targets, as well as Pat1 targets, and revealed the interplay between these two proteins in translational repression. We found that the repression of TEs often involves independent cumulative contributions by Pat1 and Dhh1, exemplified by transcripts exhibiting marked TE increases only in the double mutant. In contrast, most of the transcripts showing the strongest translational repression in WT are equally derepressed in all three mutants, indicating that Pat1 and Dhh1 must act in concert for appreciable repression of these mRNAs. Whereas ∼50% of all mRNAs translationally repressed by Dhh1 do not seem to require Pat1, those repressed by Pat1 generally exhibit some contribution from Dhh1. Thus, Dhh1 and Pat1 frequently make independent contributions to repressing translation but must cooperate extensively on the most highly repressed subset of their translational targets.

In accordance with previous findings (22), we observed that mRNAs exhibiting increased TE on elimination of Dhh1 are generally not derepressed in abundance by *dhh1Δ*. We obtained different results for Pat1, however, which represses the abundance of the mRNAs showing strong, concerted translational repression by both factors (Figure S10E). Presumably Pat1 can more readily stimulate decapping of mRNAs that it also targets for translational repression. However, most mRNAs whose abundance is repressed by Pat1 are not also translationally repressed by this factor (Figure S13E); although rapid decay could obscure translational repression.

Gene ontology analysis revealed that the non-iESR mRNAs repressed in abundance by Dhh1 or Pat1 are enriched for mRNAs encoding proteins involved in respiration (Table 1, rows 1–2). Indeed, many transcripts encoding mitochondrial Ox. Phos. proteins are derepressed in the *pat1Δ, dhh1Δ,* and *pat1Δdhh1Δ* mutants; as are mRNAs encoding components of the glyoxylate cycle and glucose-repressed (CCR) proteins needed for utilization of non-fermentable carbon sources. The derepression of selected mitochondrial proteins was confirmed by western blot analysis, and by demonstrating increased ETC activity that elevates mitochondrial membrane potential in *pat1Δ* and *dhh1Δ* cells. We found no evidence, however, for increased transcriptional activation of Ox. Phos. genes by the Hap complex, or of CCR genes by Adr1, in the decapping mutants. Thus, post-transcriptional repression by Pat1 and Dhh1 helps to suppress pathways for utilization of non-preferred carbon sources and respiration in glucose-rich medium. As noted earlier, several glucose-repressed mRNAs were found to be more rapidly degraded on addition of glucose to cells growing in a non-fermentable carbon source (6) (57) in a manner involving Xrn1 and Dhh1 (7,8). This might explain our findings that many CCR mRNAs are derepressed in the *pat1Δ, dhh1Δ* and *pat1Δdhh1Δ* mutants growing continuously on glucose if we assume that Pat1 participates with Dhh1 in this control of mRNA stability.

It was shown previously that the RNA binding protein Puf3 represses the abundance of certain mRNAs encoding mitochondrial proteins involved in respiration by enhancing their deadenylation and decapping in glucose-grown cells (58,59). Among 91 mRNAs identified as high-confidence targets of Puf3 binding and whose protein products are derepressed in *puf3Δ* cells during fermentative growth, 84 are mitochondrial proteins that support the synthesis or assembly of the complexes of Ox. Phos., while only two (Atp1 and Atp18) are Ox. Phos. proteins *per se* (60). None of the transcripts whose products function directly in Ox. Phos. found here to be derepressed by *pat1Δ* or *dhh1Δ* belong to the group of 91 high-confidence Puf3 targets, suggesting that Puf3 does not directly mediate the repressive effects of Pat1 and Dhh1 on these transcripts. How-

ever, ∼50% of the 89 non-Ox. Phos. mRNAs bound and repressed by Puf3 (60) do exhibit increased RPF abundance in *dhh1Δ* or *pat1Δ* cells, making them candidates for enhanced decapping or translational repression via Puf3-mediated recruitment of Dhh1 or Pat1. Perhaps one of the other five yeast Puf proteins (61) is involved in regulating Ox. Phos. mRNAs and numerous other transcripts repressed by Pat1/Dhh1 that do not appear to bind Puf3.

We observed increased abundance of many mRNAs subject to nitrogen catabolite repression, and both elevated abundance and TEs of mRNAs required for utilization of the non-preferred nitrogen source allantoin (Table 1, rows 1–2), all of which are normally repressed on rich YPD medium. These NCR genes are transcriptionally activated by Gln3 or Gat1 in poor nitrogen sources; however, we detected no increase in transcriptional activation by these GATA factors, nor increased Pol II occupancies of the NCR genes, in the *dhh1Δ* or *pat1Δ* mutants. Many genes required for autophagy—a pathway suppressed by abundant nitrogen—are also derepressed in the *pat1Δ, dhh1Δ* and *pat1Δdhh1Δ* mutants, and we provided evidence that low-level autophagy occurs inappropriately on rich YPD medium in these mutants. Our results suggest a more extensive repression of *ATG* transcripts than described previously (9) and implicate Pat1 in suppressing autophagy in rich medium. Finally, mRNAs translationally repressed by Pat1 or Dhh1 are enriched for transcripts encoding cell wall and membrane-anchored proteins, including those involved in cell-cell adhesion. Pat1 represses the agglutinin genes *FLO1, -5, -9* and *-11,* and we recently presented evidence that Dcp2 and Pat1 repress invasive growth in agar on rich medium (Vijjamarri et al. bioRxiv 2023.01.05.522830), a behavior dependent on cell adhesion molecules normally repressed in nutrient-replete cells.

In summary, our results demonstrate widespread cooperation between Dhh1 and Pat1 in controlling mRNA abundance, which occurs primarily via decapping by Dcp1/Dcp2 and attendant mRNA degradation versus indirect transcriptional responses. These mRNAs are generally not poorly translated nor enriched for non-optimal codons, implying a more specific targeting mechanism. Our results further demonstrate that Pat1 cooperates with Dhh1 in repressing the translation of particular mRNAs. Importantly, we found that Dhh1 and Pat1 collaborate in nutrient-replete cells to preferentially repress the abundance or translation of mRNAs encoding proteins normally expressed only in starved cells, identifying a layer of post-transcriptional control that complements known transcriptional mechanisms for coupling gene expression to nutrient availability.

DATA AVAILABILITY

Ribosome profiling, RNA-Seq, ChIP-Seq and CAGE-Seq data discussed in this publication have been deposited in NCBI's Gene Expression Omnibus and are accessible through GEO Series accession number GSE220578, https://www.ncbi.nlm.nih.gov/geo/query/acc.cgi?acc=GSE220578; GSE216831, https://www.ncbi.nlm.nih.gov/geo/query/acc.cgi?acc=GSE216831 and GSE224774, https://www.ncbi.nlm.nih.gov/geo/query/acc.cgi?acc=GSE224774. TMT-MS/MS proteomics raw data have been deposited in ProteomeXchange with the accession numbers PXD042828 and PXD042990. Previously published datasets used in the study can be found at 10.1371/journal.pgen.1008299 (23).

SUPPLEMENTARY DATA

Supplementary Data are available at NAR Online.

ACKNOWLEDGEMENTS

We are grateful to Feng He, Allan Jacobson and Bertrand Séraphin for gifts of yeast strains, Nikolaus Pfanner and Thomas Fox for gifts of antibodies, Henry Zhang for help with bioinformatics and the NHLBI Proteomics Core for TMT-MS/MS analysis. We thank Jon Lorsch for financial support of DNA sequencing and invaluable advice, and all other members of our laboratories for helpful comments and suggestions.

FUNDING

Intramural Research Program of the NIH (in part); C.O. and M.L.G. were supported by NIH grant [R01 HL117880]; X.N. and Z.L. by NSF grant [1951332]; Saint Louis University 2022 President's Research Fund. Funding for open access charge: Intramural Program of the National Institutes of Health [HD001004].
Conflict of interest statement. None declared.

REFERENCES

1. Parker,R. (2012) RNA degradation in Saccharomyces cerevisae. *Genetics*, **191**, 671–702.
2. Charenton,C., Gaudon-Plesse,C., Fourati,Z., Taverniti,V., Back,R., Kolesnikova,O., Seraphin,B. and Graille,M. (2017) A unique surface on Pat1 C-terminal domain directly interacts with Dcp2 decapping enzyme and Xrn1 5′-3′ mRNA exonuclease in yeast. *Proc. Natl. Acad. Sci. U.S.A.*, **114**, E9493–E9501.
3. Lobel,J.H., Tibble,R.W. and Gross,J.D. (2019) Pat1 activates late steps in mRNA decay by multiple mechanisms. *Proc. Natl. Acad. Sci. U.S.A.*, **116**, 23512–23517.
4. He,F., Wu,C. and Jacobson,A. (2022) Dcp2 C-terminal cis-binding elements control selective targeting of the decapping enzyme by forming distinct decapping complexes. *Elife*, **11**, e74410.
5. He,F., Celik,A., Wu,C. and Jacobson,A. (2018) General decapping activators target different subsets of inefficiently translated mRNAs. *Elife*, **7**, e34409.
6. Lombardo,A., Cereghino,G.P. and Scheffler,I.E. (1992) Control of mRNA turnover as a mechanism of glucose repression in Saccharomyces cerevisiae. *Mol. Cell. Biol.*, **12**, 2941–2948.
7. Cereghino,G.P. and Scheffler,I.E. (1996) Genetic analysis of glucose regulation in saccharomyces cerevisiae: control of transcription versus mRNA turnover. *EMBO J.*, **15**, 363–374.
8. Braun,K.A., Vaga,S., Dombek,K.M., Fang,F., Palmisano,S., Aebersold,R. and Young,E.T. (2014) Phosphoproteomic analysis identifies proteins involved in transcription-coupled mRNA decay as targets of Snf1 signaling. *Sci. Signal*, **7**, ra64.
9. Hu,G., McQuiston,T., Bernard,A., Park,Y.D., Qiu,J., Vural,A., Zhang,N., Waterman,S.R., Blewett,N.H., Myers,T.G. *et al.* (2015) A conserved mechanism of TOR-dependent RCK-mediated mRNA degradation regulates autophagy. *Nat. Cell Biol.*, **17**, 930–942.
10. Gatica,D., Hu,G., Liu,X., Zhang,N., Williamson,P.R. and Klionsky,D.J. (2019) The Pat1-Lsm complex stabilizes ATG mRNA during nitrogen starvation-induced autophagy. *Mol. Cell*, **73**, 314–324.

11. Holmes,L.E., Campbell,S.G., De Long,S.K., Sachs,A.B. and Ashe,M.P. (2004) Loss of translational control in yeast compromised for the major mRNA decay pathway. *Mol. Cell. Biol.*, **24**, 2998–3010.
12. Coller,J. and Parker,R. (2005) General translational repression by activators of mRNA decapping. *Cell*, **122**, 875–886.
13. Arribere,J.A., Doudna,J.A. and Gilbert,W.V. (2011) Reconsidering movement of eukaryotic mRNAs between polysomes and P bodies. *Mol. Cell*, **44**, 745–758.
14. Wyers,F., Minet,M., Dufour,M.E., Vo,L.T. and Lacroute,F. (2000) Deletion of the PAT1 gene affects translation initiation and suppresses a PAB1 gene deletion in yeast. *Mol. Cell. Biol.*, **20**, 3538–3549.
15. Tharun,S. and Parker,R. (2001) Targeting an mRNA for decapping: displacement of translation factors and association of the Lsm1p-7p complex on deadenylated yeast mRNAs. *Mol. Cell*, **8**, 1075–1083.
16. Sweet,T., Kovalak,C. and Coller,J. (2012) The DEAD-Box protein Dhh1 promotes decapping by slowing ribosome movement. *PLoS Biol.*, **10**, e1001342.
17. Carroll,J.S., Munchel,S.E. and Weis,K. (2011) The DExD/H box ATPase Dhh1 functions in translational repression, mRNA decay, and processing body dynamics. *J. Cell Biol.*, **194**, 527–537.
18. Presnyak,V., Alhusaini,N., Chen,Y.H., Martin,S., Morris,N., Kline,N., Olson,S., Weinberg,D., Baker,K.E., Graveley,B.R. *et al.* (2015) Codon optimality is a major determinant of mRNA stability. *Cell*, **160**, 1111–1124.
19. Radhakrishnan,A., Chen,Y.H., Martin,S., Alhusaini,N., Green,R. and Coller,J. (2016) The DEAD-Box protein Dhh1p couples mRNA decay and translation by monitoring codon optimality. *Cell*, **167**, 122–132.
20. Buschauer,R., Matsuo,Y., Sugiyama,T., Chen,Y.H., Alhusaini,N., Sweet,T., Ikeuchi,K., Cheng,J., Matsuki,Y., Nobuta,R. *et al.* (2020) The Ccr4-Not complex monitors the translating ribosome for codon optimality. *Science*, **368**, eaay6912.
21. Webster,M.W., Chen,Y.H., Stowell,J.A.W., Alhusaini,N., Sweet,T., Graveley,B.R., Coller,J. and Passmore,L.A. (2018) mRNA deadenylation is coupled to translation rates by the differential activities of Ccr4-Not nucleases. *Mol. Cell*, **70**, 1089–1100.
22. Jungfleisch,J., Nedialkova,D.D., Dotu,I., Sloan,K.E., Martinez-Bosch,N., Bruning,L., Raineri,E., Navarro,P., Bohnsack,M.T., Leidel,S.A. *et al.* (2017) A novel translational control mechanism involving RNA structures within coding sequences. *Genome Res.*, **27**, 95–106.
23. Zeidan,Q., He,F., Zhang,F., Zhang,H., Jacobson,A. and Hinnebusch,A.G. (2018) Conserved mRNA-granule component Scd6 targets Dhh1 to repress translation initiation and activates Dcp2-mediated mRNA decay in vivo. *PLos Genet.*, **14**, e1007806.
24. Liu,X., Yao,Z., Jin,M., Namkoong,S., Yin,Z., Lee,J.H. and Klionsky,D.J. (2019) Dhh1 promotes autophagy-related protein translation during nitrogen starvation. *PLoS Biol.*, **17**, e3000219.
25. Love,M.I., Huber,W. and Anders,S. (2014) Moderated estimation of fold change and dispersion for RNA-seq data with DESeq2. *Genome Biol.*, **15**, 550.
26. Schmitt,M.E., Brown,T.A. and Trumpower,B.L. (1990) A rapid and simple method for preparation of RNA from Saccharomyces cerevisiae. *Nucleic Acids Res.*, **18**, 3091–3092.
27. Murata,M., Nishiyori-Sueki,H., Kojima-Ishiyama,M., Carninci,P., Hayashizaki,Y. and Itoh,M. (2014) Detecting expressed genes using CAGE. *Methods Mol. Biol.*, **1164**, 67–85.
28. Kim,D., Paggi,J.M., Park,C., Bennett,C. and Salzberg,S.L. (2019) Graph-based genome alignment and genotyping with HISAT2 and HISAT-genotype. *Nat. Biotechnol.*, **37**, 907–915.
29. Lu,Z., Berry,K., Hu,Z., Zhan,Y., Ahn,T.H. and Lin,Z. (2021) TSSr: an R package for comprehensive analyses of TSS sequencing data. *NAR Genom Bioinform*, **3**, lqab108.
30. Lu,Z. and Lin,Z. (2021) The origin and evolution of a distinct mechanism of transcription initiation in yeasts. *Genome Res.*, **31**, 51–63.
31. Qiu,H., Chereji,R.V., Hu,C., Cole,H.A., Rawal,Y., Clark,D.J. and Hinnebusch,A.G. (2016) Genome-wide cooperation by HAT Gcn5, remodeler SWI/SNF, and chaperone Ydj1 in promoter nucleosome eviction and transcriptional activation. *Genome Res.*, **26**, 211–225.
32. Langmead,B., Trapnell,C., Pop,M. and Salzberg,S.L. (2009) Ultrafast and memory-efficient alignment of short DNA sequences to the human genome. *Genome Biol.*, **10**, R25.
33. Robinson,J.T., Thorvaldsdottir,H., Winckler,W., Guttman,M., Lander,E.S., Getz,G. and Mesirov,J.P. (2011) Integrative genomics viewer. *Nat. Biotechnol.*, **29**, 24–26.
34. Zecha,J., Satpathy,S., Kanashova,T., Avanessian,S.C., Kane,M.H., Clauser,K.R., Mertins,P., Carr,S.A. and Kuster,B. (2019) TMT labeling for the masses: a robust and cost-efficient, in-solution labeling approach. *Mol. Cell. Proteomics*, **18**, 1468–1478.
35. Reid,G.A. and Schatz,G. (1982) Import of proteins into mitochondria. Yeast cells grown in the presence of carbonyl cyanide m-chlorophenylhydrazone accumulate massive amounts of some mitochondrial precursor polypeptides. *J. Biol. Chem.*, **257**, 13056–13061.
36. Nanda,J.S., Cheung,Y.N., Takacs,J.E., Martin-Marcos,P., Saini,A.K., Hinnebusch,A.G. and Lorsch,J.R. (2009) eIF1 controls multiple steps in start codon recognition during eukaryotic translation initiation. *J. Mol. Biol.*, **394**, 268–285.
37. Bushman,J.L., Asuru,A.I., Matts,R.L. and Hinnebusch,A.G. (1993) Evidence that GCD6 and GCD7, translational regulators of *GCN4* are subunits of the guanine nucleotide exchange factor for eIF-2 in *Saccharomyces cerevisiae*. *Mol. Cell. Biol.*, **13**, 1920–1932.
38. Ingolia,N.T., Ghaemmaghami,S., Newman,J.R. and Weissman,J.S. (2009) Genome-wide analysis in vivo of translation with nucleotide resolution using ribosome profiling. *Science*, **324**, 218–223.
39. O'Duibhir,E., Lijnzaad,P., Benschop,J.J., Lenstra,T.L., van Leenen,D., Groot Koerkamp,M.J., Margaritis,T., Brok,M.O., Kemmeren,P. and Holstege,F.C. (2014) Cell cycle population effects in perturbation studies. *Mol. Syst. Biol.*, **10**, 732.
40. Gasch,A.P., Spellman,P.T., Kao,C.M., Carmel-Harel,O., Eisen,M.B., Storz,G., Botstein,D. and Brown,P.O. (2000) Genomic expression programs in the response of yeast cells to environmental changes. *Mol. Biol. Cell*, **11**, 4241–4257.
41. Hu,W., Sweet,T.J., Chamnongpol,S., Baker,K.E. and Coller,J. (2009) Co-translational mRNA decay in *Saccharomyces cerevisiae*. *Nature*, **461**, 225–229.
42. Pelechano,V., Wei,W. and Steinmetz,L.M. (2015) Widespread co-translational RNA decay reveals ribosome dynamics. *Cell*, **161**, 1400–1412.
43. Pelechano,V., Wei,W. and Steinmetz,L.M. (2013) Extensive transcriptional heterogeneity revealed by isoform profiling. *Nature*, **497**, 127–131.
44. Sun,M., Schwalb,B., Pirkl,N., Maier,K.C., Schenk,A., Failmezger,H., Tresch,A. and Cramer,P. (2013) Global analysis of eukaryotic mRNA degradation reveals Xrn1-dependent buffering of transcript levels. *Mol. Cell*, **52**, 52–62.
45. Elfving,N., Chereji,R.V., Bharatula,V., Bjorklund,S., Morozov,A.V. and Broach,J.R. (2014) A dynamic interplay of nucleosome and Msn2 binding regulates kinetics of gene activation and repression following stress. *Nucleic Acids Res.*, **42**, 5468–5482.
46. Thompson,M.K., Rojas-Duran,M.F., Gangaramani,P. and Gilbert,W.V. (2016) The ribosomal protein Asc1/RACK1 is required for efficient translation of short mRNAs. *Elife*, **5**, e11154.
47. Costello,J., Castelli,L.M., Rowe,W., Kershaw,C.J., Talavera,D., Mohammad-Qureshi,S.S., Sims,P.F., Grant,C.M., Pavitt,G.D., Hubbard,S.J. *et al.* (2015) Global mRNA selection mechanisms for translation initiation. *Genome Biol.*, **16**, 10.
48. Sabi,R. and Tuller,T. (2014) Modelling the efficiency of codon-tRNA interactions based on codon usage bias. *DNA Res.*, **21**, 511–526.
49. Young,E.T., Dombek,K.M., Tachibana,C. and Ideker,T. (2003) Multiple pathways are co-regulated by the protein kinase Snf1 and the transcription factors Adr1 and Cat8. *J. Biol. Chem.*, **278**, 26146–26158.
50. Tachibana,C., Yoo,J.Y., Tagne,J.B., Kacherovsky,N., Lee,T.I. and Young,E.T. (2005) Combined global localization analysis and transcriptome data identify genes that are directly coregulated by Adr1 and Cat8. *Mol. Cell. Biol.*, **25**, 2138–2146.
51. Broach,J.R. (2012) Nutritional control of growth and development in yeast. *Genetics*, **192**, 73–105.
52. Sloan,J.S., Dombek,K.M. and Young,E.T. (1999) Post-translational regulation of Adr1 activity is mediated by its DNA binding domain. *J. Biol. Chem.*, **274**, 37575–37582.
53. Forsburg,S.L. and Guarente,L. (1989) Identification and characterization of HAP4: a third component of the CCAAT-bound HAP2/HAP3 heteromer. *Genes Dev.*, **3**, 1166–1178.

54. Godard,P., Urrestarazu,A., Vissers,S., Kontos,K., Bontempi,G., van Helden,J. and Andre,B. (2007) Effect of 21 different nitrogen sources on global gene expression in the yeast Saccharomyces cerevisiae. *Mol. Cell. Biol.*, **27**, 3065–3086.
55. Reggiori,F. and Klionsky,D.J. (2013) Autophagic processes in yeast: mechanism, machinery and regulation. *Genetics*, **194**, 341–361.
56. Miller,J.E., Zhang,L., Jiang,H., Li,Y., Pugh,B.F. and Reese,J.C. (2018) Genome-wide mapping of decay factor-mRNA interactions in yeast identifies nutrient-responsive transcripts as targets of the deadenylase Ccr4. *G3 (Bethesda)*, **8**, 315–330.
57. Young,E.T., Zhang,C., Shokat,K.M., Parua,P.K. and Braun,K.A. (2012) The AMP-activated protein kinase Snf1 regulates transcription factor binding, RNA polymerase II activity, and mRNA stability of glucose-repressed genes in *Saccharomyces cerevisiae*. *J. Biol. Chem.*, **287**, 29021–29034.
58. Olivas,W. and Parker,R. (2000) The Puf3 protein is a transcript-specific regulator of mRNA degradation in yeast. *EMBO J.*, **19**, 6602–6611.
59. Miller,M.A., Russo,J., Fischer,A.D., Lopez Leban,F.A. and Olivas,W.M. (2014) Carbon source-dependent alteration of Puf3p activity mediates rapid changes in the stabilities of mRNAs involved in mitochondrial function. *Nucleic Acids Res.*, **42**, 3954–3970.
60. Lapointe,C.P., Stefely,J.A., Jochem,A., Hutchins,P.D., Wilson,G.M., Kwiecien,N.W., Coon,J.J., Wickens,M. and Pagliarini,D.J. (2018) Multi-omics reveal specific targets of the RNA-binding protein Puf3p and its orchestration of mitochondrial biogenesis. *Cell Syst.*, **6**, 125–135.
61. Quenault,T., Lithgow,T. and Traven,A. (2011) PUF proteins: repression, activation and mRNA localization. *Trends Cell Biol.*, **21**, 104–112.